NTNU

Norwegian University of
Science and Technology

Radiation dose and image quality in CT

Evaluation of how slice thickness, tube current modulation and reconstruction algorithms affect radiation dose and image noise

Marte Anette Dunseth Guleng

Master of Science
Submission date: June 2018
Supervisor: Kathrine Røe Redalen, IFY
Co-supervisor: Kirsten Nygaard Bolstad, Haukeland universitetssjukehus

Norwegian University of Science and Technology
Department of Physics

Abstract

Background. Helse Vest has currently standardized the computed tomography (CT) Thorax/Abdomen/Pelvis protocols in the region. One of the standardized parameters was a reduction of the reconstructed slice thickness from 5 mm to 3 mm. Brooks' formula, which describes the relationship between radiation dose, image noise and slice thickness in CT, has been used to estimate the effects of the slice thickness reduction on radiation dose and image noise. Exposure parameters like the tube voltage (kV) and tube current-time product (mAs) are currently not standardized.

Aim. The aim of this thesis was to investigate the effects of reducing the reconstructed image slice thickness for CT Thorax/Abdomen/Pelvis protocols in Helse Vest. This was done by investigating how slice thickness, automatic tube current modulation (ATCM) and reconstruction algorithms affects radiation dose and image noise on four different CT scanners, and compare the results with the estimates made by Brooks' formula.

Materials and methods. An ATCM phantom was scanned with Thorax/Abdomen/Pelvis protocols on four CT scanners from GE, Philips, Siemens and Toshiba. The protocols were based on recommendations from the American Association of Physicists in Medicine (AAPM). Scans were performed both with a reconstructed slice thickness of 5 mm, and while keeping either the radiation dose or image noise constant when reducing the slice thickness from 5 mm to 3 mm. The radiation dose and image noise was kept at the desired level by adjusting the ATCM index for each scanner according to Brooks' formula. All images were reconstructed with both filtered back projection (FBP) and iterative reconstruction (IR). The obtained image series were analyzed with respect to dose by looking at the volume CT dose index (CTDI_{vol}) and mAs, and with respect to image noise by looking at the standard deviation (SD) noise in the z-direction, noise power spectrum (NPS) curves and inter-image SD noise maps.

Results. The changes in radiation dose and image noise caused by the slice thickness reduction appeared as predicted by Brooks' formula, and the changes were similar when using both FBP and IR. When comparing a single protocol reconstructed with FBP and IR, the use of IR reduced the radiation dose on GE, and reduced the image noise on Philips, Siemens and Toshiba. When using IR on Toshiba, the amount of noise reduction performed by the IR algorithm was adapted according to the amount of noise present in the image. Toshiba applied the chosen ATCM index to a pre-defined slice thickness of 5 mm, regardless of the reconstructed slice thickness chosen by the operator.

Conclusion. When image slice thickness was reduced in CT protocols, Brooks' formula provided reliable predictions for the behavior of radiation dose and image noise, both when using FBP and IR as reconstruction methods. Due to differences found for different vendors, Helse Vest should, if they wish to further standardize the exposure parameters for their CT Thorax/Abdomen/Pelvis protocols, proceed carefully and pay particular attention to how the IR algorithms behave on the different scanners, and how each scanner applies the input exposure parameters.

Sammendrag

Bakgrunn. Helse Vest har nylig standardisert computertomografi (CT) Thorax/Abdomen/Bekken protokoller som brukes i regionen. En av parametrene som har blitt standardisert er den rekonstruerte bildesnittykkelsen, som har blitt redusert fra 5 mm til 3 mm. Brooks' formel, som beskriver forholdet mellom stråledose, bildestøy og snittykkelse i CT, har blitt brukt for å anslå hvilken effekt den reduserte snittykkelsen vil ha for stråledose og bildestøy. Eksponeringsparametre som rørspenning (kV) og produktet av rørstrøm og rotasjonstid (mAs) har foreløpig ikke blitt standardisert.

Formål. Formålet med denne oppgaven var å undersøke effekten av å redusere den rekonstruerte snittykkelsen for CT Thorax/Abdomen/Bekken protokoller i Helse Vest. Dette ble gjort ved å se på hvordan snittykkelse, automatisk dosemodulering (automatic tube current modulation; ATCM) og rekonstruksjonsalgoritmer påvirker stråledose og bildestøy på fire forskjellige CT-scannere, og å sammenligne resultatet med anslagene gjort med Brooks' formel.

Materialer og metoder. Et ATCM-fantom ble scannet med Thorax/Abdomen/Bekken protokoller på fire CT-scannere fra GE, Philips, Siemens og Toshiba. Protokollene var basert på anbefalinger fra American Association of Physicists in Medicine (AAPM). Det ble scannet både med en rekonstruert snittykkelse på 5 mm, og med enten konstant stråledose eller konstant bildestøy når snittykkelsen ble redusert fra 5 mm til 3 mm. Stråledosen og bildestøyen ble holdt på ønsket nivå ved å justere ATCM-indeksen for hver scanner etter Brooks' formel. Alle bildeserier ble rekonstruert både med filtrert tilbakeprojeksjon (FBP) og iterativ rekonstruksjon (IR). Stråledosen i hver bildeserie ble analysert ved å se på volum CT doseindeks (CTDI_{vol}) og mAs, og bildestøyen ble analysert ved å se på støy som standardavvik (SD) langs z-retning, kurver for støyeffektspektrum (noise power spectrum; NPS), og støykart.

Resultater. Reduksjon i bildesnittykkelse førte til endringer i stråledose og bildestøy som stemte overens med Brooks' formel, og lignende endringer ble funnet ved bruk av både FBP og IR. Ved å sammenligne en gitt protokoll rekonstruert med FBP og IR, ga bruk av IR en dosebesparelse på GE, og en støyreduksjon på Philips, Siemens og Toshiba. Når IR ble brukt på Toshiba, ble mengden støyreduksjon justert etter mengden støy til stede i bildet. Toshiba anvendte den valgte ATCM-indeksen på en forhåndsdefinert snittykkelse på 5 mm, uavhengig av den rekonstruerte snittykkelsen valgt av operatør.

Konklusjon. Når bildesnittykkelsen i en CT-protokoll ble redusert, ga Brooks' formel et troverdig estimat av stråledose og bildestøy, både ved bruk av FBP og IR som rekonstruksjonsmetoder. På grunn av forskjeller mellom de ulike leverandørene, bør Helse Vest tre forsiktig frem dersom de ønsker å ytterligere standardisere eksponeringsparametre for CT Thorax/Abdomen/Bekken-protokoller. De bes å legge spesielt merke til hvordan de forskjellige IR algoritmene oppfører seg på ulike scannere, og hvordan hver scanner appliserer de valgte eksponeringsparametrene.

Preface

The following thesis is written as part of the five year master's program in Natural Science with Teacher Education (Lektorutdanning i realfag) at the Norwegian University of Science and Technology (NTNU). The thesis was carried out at the Department of Physics during the spring of 2018, and marks the end of my studies at NTNU. The experimental work has been carried out at Haukeland University Hospital (HUS) in Bergen.

I would like to thank my internal supervisor at the Department of Physics at NTNU, Kathrine Røe Redalen, for including me in her research group, being available for questions and guidance, and for making sure all the formal aspects of my degree are in order.

A great thanks is also due to all the people at HUS who have helped make this thesis a reality. First and foremost, thank you to my supervisor at HUS, Kirsten Nygaard Bolstad, for giving me the opportunity to experience a physicist's life at the hospital. You have provided solid support through all phases of this project. Thank you for sharing generously of your ideas and expertise, for being available when needed, for your encouragements, and for being utterly thorough and constructive in your feedback.

Thank you also to physicists at HUS Daniel Aadnevik, Ingvild Dalehaug and Silje Flatabø. You have all been very helpful with measurements at the labs, sharing your knowledge, ideas and suggestions, and also in giving me feedback on my work. For this I am truly grateful. And without the programs developed by Helge Pettersen, also a physicist at HUS, I would still be sorting DICOM files, not to mention that the noise maps would not exist. Thank you so much for lending your expertice to this thesis. I am overall very grateful for having been given the opportunity to write for Haukeland, thank you all for being such nice people!

As five years of education now draws to a close, I would like to use this opportunity to express my gratitute to my family. To my parents and my grandparents: Thank you for promoting the importance of education, and for encouraging and supporting my pursuit of it. Thank you for giving me freedom to decide for myself. You cannot choose your family, but I would've chosen you every time.

And last but not least, to Vegar, whose heroic deeds exceeds the scope of this thesis: Thank you for making every day that much more enjoyable. You are the best.

Anette Guleng
Trondheim, May 2018

Table of Contents

Abbreviations

AAPM	=	American Association of Physicists in Medicine
ADMIRE	=	Advanced Modeled Iterative Reconstruction (IR system from Siemens)
AIDR	=	Adaptive Iterative Dose Reduction (IR system from Toshiba)
ALARA	=	As low as reasonably achievable
ASIR-V	=	Adaptive Statistical Iterative Reconstruction - Veo (IR system from GE)
ATCM	=	Automatic tube current modulation
BW	=	Beam width
CT	=	Computed tomography
CTDI	=	Computed tomography dose index
DICOM	=	Digital imaging and communications in medicine
DLP	=	Dose-length product
DRI	=	DoseRight Index
FBP	=	Filtered back projection
FOV	=	Field of view
HDS	=	Haraldsplass Diakonale Sykehus (Haraldsplass Diaconal Hospital)
HU	=	Hounsfield unit
HUS	=	Haukeland universitetssjukehus (Haukeland university hospital)
IR	=	Iterative reconstruction
KiH	=	Kysthospitalet i Hagevik (the Coastal hospital in Hagevik)
kVp	=	Kilo-volt peak
LNT	=	Linear no-threshold
MRI	=	Magnetic resonance imaging
NI	=	Noise index
NPS	=	Noise power spectrum
QRM	=	Quality reference mAs
RERF	=	Radiation Effects Research Forum
ROI	=	Region of interest
SD	=	Standard deviation
SPR	=	Scanned projection radiograph
TF	=	Table feed
WL	=	Window level
WW	=	Window width

Chapter 1

Introduction

The ability to use radiation to create images of the inside of the human body has revolutionized the medical field, and medical imaging technology has become an indispensable tool in diagnostic medicine. X-rays are widely utilized in a variety of procedures, like taking an image of a broken bone, performing a long-lasting interventional procedure with real-time x-ray image guidance to remove blood clots in the patient's intracranial vessels, or creating slices and three-dimensional images of the body with computed tomography (CT). While the use of radiation in many cases is life-saving, there is also a risk involved. Ionizing radiation, like x-rays, may damage the cells of the body. This can lead to acute damage, like skin damage and hair loss, and possibly carcinogenic effects. A CT scan involves a high radiation risk, because the dose to the patient is high compared to other imaging modalities [1]. This gives radiation professionals a responsibility to optimize each procedure, so that the benefits from the obtained image information will outweigh the risk involved.

Helse Vest, or the Western Norway Regional Health Authority, is one of four regional health authorities in Norway. It holds responsibility for operating hospitals located in the counties of Sogn og Fjordane, Hordaland and Rogaland, through the hospital trusts in Førde, Bergen, Fonna and Stavanger. The hospital trusts in Helse Vest can be seen in Figure 1.1. Several standardization projects are currently ongoing in the region, with the aim to provide "the right diagnostics at the right time". One step in achieving this goal, is to work on harmonizing the guidelines for radiologic procedures between the hospital trusts in the region. By standardizing examination procedures, a patient will not need to perform a second examinations because the same procedure is performed in different ways at two different hospitals. This will improve the utilization of resources in the region, and avoid unnecessary risk from radiation exposure to the patient. Standardization is prioritized for procedures that give high radiation doses, like CT, and for modalities where the capacity is limited, like magnetic resonance imaging (MRI). The standardization projects involve radiologists and radiographers from each hospital in Helse Vest as participants, in addition to a physicist.

As a result of the standardization projects in Helse Vest, several detailed changes have

Figure 1.1: A map showing Helse Vest (the Western Norway Regional Health Authority) with its four health trusts: Helse Førde, Helse Bergen, Helse Fonna and Helse Stavanger. Hospitals in the region are marked. Map from [2].

been made pertaining to the acquisition and reconstruction of CT images. This involves guidelines for the reformatting of images along the coronal, sagittal, axial and other angular planes, and reducing the image slice thickness from 5 mm to 3 mm for many CT protocols. One such protocol is the CT Thorax/Abdomen/Pelvis, which is one of the most commonly used protocols at HUS. Its use includes follow-up of cancer patients, which necessitates a sufficient image quality for early detection of possible metastasis, while at the same time keeping the radiation dose low, since the patient will be performing the examination several times.

A reduction of slice thickness may affect both the patient's radiation dose and the image quality, and estimates have been made to predict the effect of reducing the slice thickness from 5 to 3 mm. The estimates were done with a formula known as "Brooks' formula", that takes into account the relationship between radiation dose, attenuation in the object, image noise, slice thickness and sample increment and -width. Brooks' formula assumes filtered back projection (FBP) as a reconstruction technique, which has been used in CT since the introduction of the CT scanner in the early 1970s. In all newer CT scanners a second reconstruction technique is also available, namely iterative reconstruction (IR),

which reduces image noise.

The aim of this thesis was to evaluate the behavior of radiation dose and image noise when the image slice thickness in CT is reduced from 5 to 3 mm. To obtain an objective basis for comparing the performance of each scanner, the protocols used were based on recommendations from the American Association of Physicists in Medicine (AAPM) [3]. First, the automatic tube current modulation (ATCM) systems implemented in four CT scanners from different vendors were evaluated, to see if the increase in dose behaves according to Brooks' formual when the image slice thickness is reduced and the image noise is kept unchanged. Second, the image noise level was evaluated for the same scanners, to see if the increase in noise behaves according to Brooks' formula when the image slice thickness is reduced and the radiation dose is kept unchanged. This was done using both FBP and IR as reconstruction methods.

Chapter 2

Theory

Computed tomography (CT) is an imaging modality that utilizes the attenuation of x-rays in the body to create images. High-attenuating tissue in the body, such as bone, will absorb more of the incoming x-rays, while low-attenuating tissue, such as the lungs, will let more radiation pass through. In traditional projection radiography, all structures in the irradiated area are superimposed in the resulting image, i.e. showing all structures on top of each other without any information about the depth of the different structures. In modern CT scanners on the other hand, a cone shaped beam irradiates the desired area from multiple angles 360°around the patient, making it possible to create a two-dimensional cross-sectional image of the body. For this reason, the term 'computed tomography' is partly derived from the greek word 'tomos', meaning 'slice' or 'section' [4].

Great work was done in developing the CT imaging technique in the 1960s and 1970s, and the first CT prototype was made by Sir Godfrey Hounsfield in 1971, with the first clinical scan published in 1972 [5]. Hounsfield, together with Allan MacLeod Cormac, won the Nobel Prize for medicine in 1979 for their work with this technology. The use of CT revolutionized the field of medical imaging, and greatly advanced the diagnostic possibilities in medicine. CT scanners are now widely utilized all over the world, and are used as a standard diagnostic tool.

While CT has become an indispensable tool in medicine, it also gives a high radiation dose during an examination. This is evident from the fact that CT scans only accounted for 21% of medical imaging examinations in Norway in 2008, while it accounted for as much as 80% of the collective dose given from medical examinations in the same period (compared with conventional x-ray, ultrasound and MRI) [1]. For this reason it is important that a CT examination is justified, i.e. that the benefits from the obtained information outweighs the risks of the radiation exposure, and that the procedure is optimized to keep the patient dose As Low As Reasonably Achievable (the ALARA principle).

2.1 Radiation-induced cancer risk

The biologic effects caused by x-rays are a result of DNA damage inflicted on the cells of the body. X-ray radiation can damage the DNA directly, by setting fast-moving charged particles in motion that cause ionizations in the DNA, or the damage can be inflicted indirectly, by free radicals created by the incoming radiation that drift to and react with the DNA chain [6].

If the DNA damage from one single high dose exposure is not repaired, the affected cells could die or lose their ability to proliferate. This is the cause of acute, or deterministic, radiation effects like erythema and epilation [6]. Some cells can still be viable after sustaining damage, and continue to live and proliferate in a mutated condition. These cells can cause carcinogenic effects, resulting in the development of cancer. Carcinogenesis is a so-called stochastic effect, meaning that an increase in received dose will increase the *risk* of the effect to occur, while the severity of the effect remains constant [6].

The Radiation Effects Research Foundation (RERF) have used data from atomic bomb survivors in Japan to study the relationship between high radiation doses (>100 mSv) and cancer risk. They have found that at high dose levels, the risk of radiation induced cancer increases linearly with dose when displayed in a log-lin plot [7]. Thus, the additional risk imposed by a radiation event is independent of the amount of radiation already received. The dose-risk relationship is more uncertain for lower radiation doses (<100 mSv), and several models have been developed to describe it. One of these models is the linear no-threshold (LNT) model, which extrapolates the linearity from high doses and applies it to low doses as well. The model thus presents the dose-risk relationship as a linear curve, with the same slope for both low and high doses. In this context, the doses given from radiologic procedures lie in the low-dose region, with doses well below 100 mSv. Table 2.1 shows the effective dose in mSv for some radiologic procedures, both with conventional projection radiography and CT.

Table 2.1: Typical values for some radiological procedures, based on average values of diagnostic reference levels in Norway. Data from [8].

Procedure	Effective dose [mSv]
Thorax	0.08
Pelvis	0.5
Abdomen	1.3
CT Thorax	4.7
CT Abdomen/Pelvis	9.5

Figure 2.1 shows the LNT model, together with other possible dose-risk relationships for low doses. The LNT model suggests that carcinogenic effects have no dose threshold, meaning that the probability of carcinogenic effects to occur will always be greater than zero for any radiation exposure, even at low doses [6].

Since CT is a modality associated with large radiation doses compared to other imaging modalities, it also involves a greater risk of developing radiation induced cancer. Still, a CT scan will in many cases be life saving for the patient. It is important that the benefits of the obtained image data will outweigh the risks involved, and that each procedure is

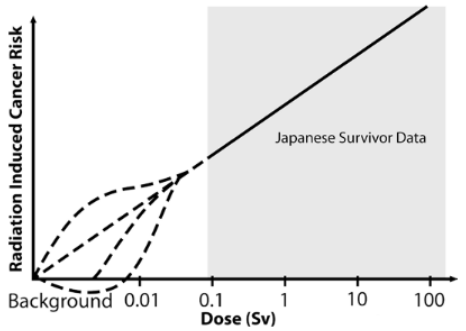

Figure 2.1: A linear no-threshold (LNT) relationship between radiation induced cancer risk and received dose will follow the dashed straight line. For doses lower than 100 mSv the dose-risk relationship is uncertain, and other models than the LNT could be more accurate. Figure from [7].

optimized according to the ALARA principle.

2.2 The CT scanner

An illustration of a CT scanner is shown in Figure 2.2. The x-ray photons utilized by the scanner are produced by an x-ray tube. In the tube, a heated metal cathode emits electrons, and the number of electrons emitted will increase with the tube current (mA). The electrons are accelerated by the accelerating voltage (kV) over the tube towards a metal target [9]. When the electrons hit the target, some of their energy are converted into x-rays, while the rest dissipates as heat. The maximum photon energy is referred to as the kilovolt peak (kVp), and occurs if the entire energy of an electron is transformed into a

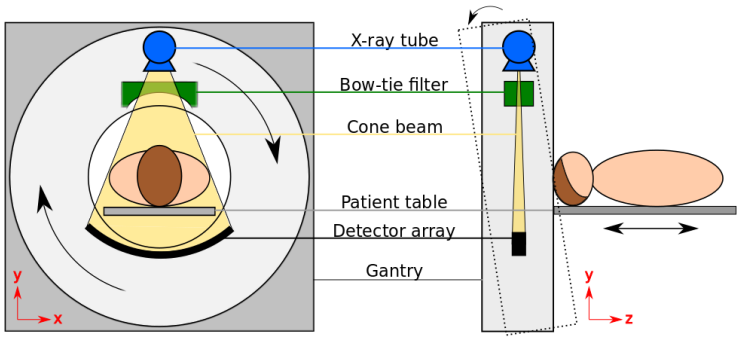

Figure 2.2: In a CT scanner, a patient is irradiated with a cone beam from an x-ray tube. The radiation passes through a bow-tie filter, and is detected by the detector array at the opposite side of the patient. The tube, filter and detector array rotates around the patient to produce slice images. The patient table can move along the z-direction to position the patient correctly in the beam. In some CT-scanners the gantry itself can be tilted at an angle.

single photon. Newer tubes have become increasingly improved with better capacities for x-ray generation.

The scanner uses a cone shaped beam, with a diameter at the isocenter of up to 70 cm in the x- and y-direction (depending on the tube angle). This diameter is called the field of view (FOV). The FOV is wide enough to cover the width of the patient in a single beam, so that the entire patient volume will be included in the image. In the z-direction, the beam has a width of up to 16 cm.

A curved detector array is placed opposite the x-ray tube to measure the intensity of the attenuated radiation beam. The detector array determines the maximal number of image slices that can be reconstructed per tube rotation, and common configurations can be e.g. 128 slices per rotation, as for the Philips Ingenuity scanner [10], and 160 slices per rotation, as for the Toshiba Aquilion Prime scanner [11]. The thinnest slice thickness available is 0.55 mm and 0.5 mm respectively for the two scanners.

In some scanners, the gantry itself can be tilted at an angle. This is mostly used when scanning the head, and can allow the operator to avoid imaging e.g. dental fillings, which could cause artifacts (errors) in the acquired image, or to avoid irradiation of the eye lense when imaging the brain.

Low-energy photons in the radiation beam will be absorbed in the patient and not reach the detector, and will thus not contribute to the image formation. To reduce the radiation dose to the patient the beam passes through a filter, which removes this low-energy radiation. Examples of x-ray energy spectra with and without a filter are shown in Figure 2.3. In CT, the photons traversing the periphery of the patient travel a shorter distance through the body than the photons traversing the center, making the beam less attenuated at the beam edges. This effect can cause artifacts in the reconstructed image [9]. One way to compensate for this is to use a bow-tie shaped filter, which reduces the

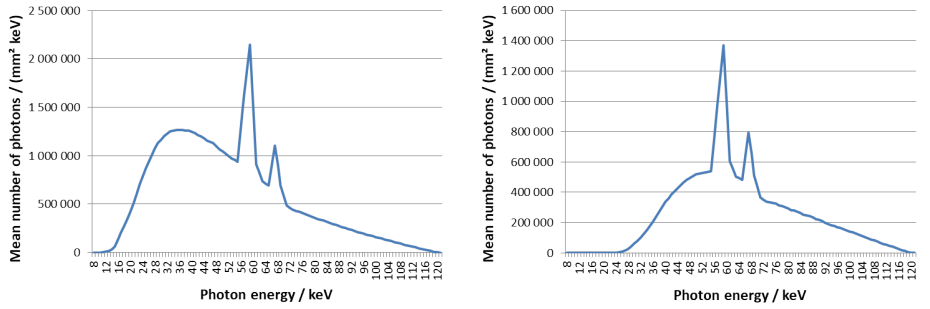

(a) Unfiltered beam

(b) Filtered beam

Figure 2.3: X-ray spectrum generated with a tungsten target material and 120 kVp for **(a)** an unfiltered beam and **(b)** a beam passing through a 0.3 mm copper filter. With a filter, the low-energy photons are removed from the spectrum, increasing the average photon energy from 52 keV in **(a)**, to 64 keV in **(b)**. The overall intensity, i.e. the number of photons reaching the irradiated object, decreases. The two distinct peaks in the spectrum are caused by photoelectric interactions, where characteristic x-rays are emitted as a target atom de-exites to fill a vacancy in the K-shell [6]. Spectra generated with [12].

intensity of the beam more at the edges than at the center. In addition to the bow-tie filter, the image reconstruction algorithms also compensate for the differences in traversed distance.

2.3 Image acquisition

During a CT scan, the patient table moves continuously as the tube performs several 360° rotations around the patient. This is called *helical scanning*, and makes the radiation beam move in a helical or spiral pattern relative to the patient. This is illustrated in Figure 2.4. The ratio of the table feed (TF), i.e. the table movement per rotation, to the beam width (BW) defines the pitch, p, for a helical scan [9]:

$$p = \frac{TF}{BW}. \tag{2.1}$$

Decreasing or increasing the pitch will either compress or extend the spiral pattern of the beam rotation, as shown in Figure 2.4.

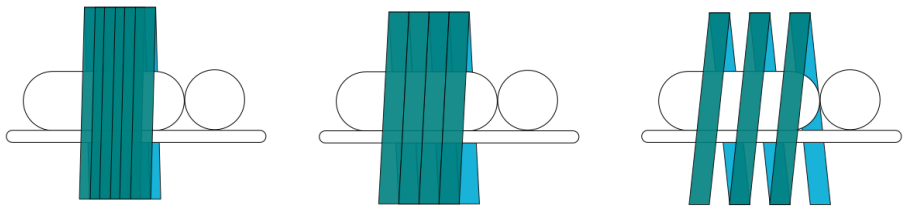

(a) $p < 1$ **(b)** $p = 1$ **(c)** $p > 1$

Figure 2.4: Helical scanning. **(a)** With $p < 1$, the radiation beam overlaps for each rotation of the tube. **(b)** With $p = 1$, the beam edges align throughout the scan. **(c)** With $p > 1$, there are gaps between the radiation beam for each tube rotation.

When a photon beam traverse the human body, the radiation will be attenuated and some of the energy absorbed by the irradiated tissue. The attenuation of a material is described by its attenuation coefficient, μ, which is dependent on the characteristics of the irradiated tissue and the energy of the x-ray beam. In a CT image, each pixel in the displayed image will represent a volume element, called a voxel ("volume pixel"), and the value in each voxel represents the average attenuation through that particular volume element. Each voxel has a width and height equal to the pixel size of the reconstructed image, and a depth equal to the slice thickness of the image.

A two-dimensional image is created from a series of one-dimensional projections [9]. The process is illustrated in Figure 2.5. A projection is obtained by irradiation from one angle. For each projection, the detector measures the attenuation profile of the irradiated area from the given angle. When several projections of the same area have been obtained from different angles, the projection data is often displayed in a sinogram. In the sinogram, the attenuation along a single projection angle is represented by a horizontal line, and the pixel values in the sinogram represent the values of the attenuation coefficients through the

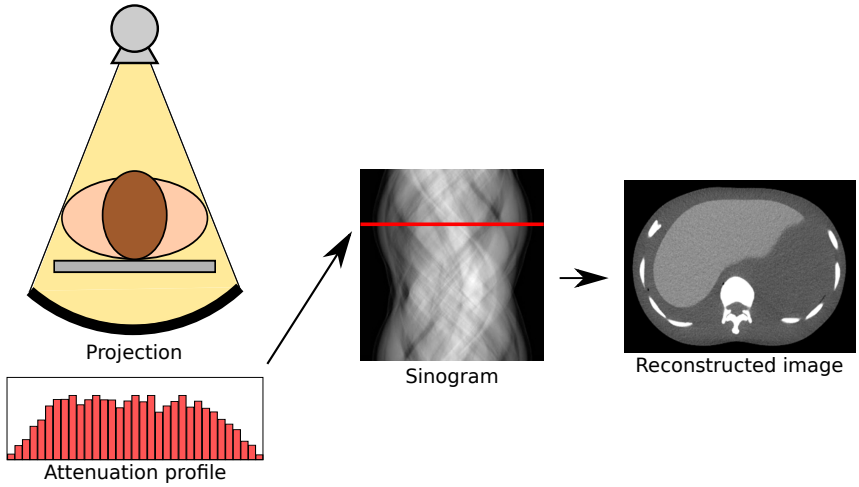

Figure 2.5: One projection measures the attenuation profile through the patient from one specific angle. Attenuation profiles from several different angles are displayed in a sinogram, where each horizontal line of pixels represents the attenuation values from one projection angle. The measured attenuation profiles can be back-projected to reconstruct a cross-section image of the irradiated volume. Sinogram from [13].

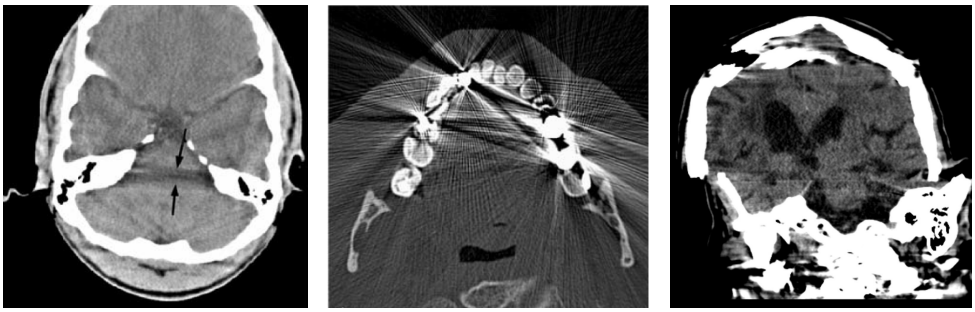

(a) Beam-hardening artifact **(b)** Metal artifact **(c)** Motion artifact

Figure 2.6: **(a)** A beam-hardening artifact (marked with arrows) appearing as a dark streak between two dense bone structures in the skull. **(b)** Metal artifacts from an image of the jaw, caused by amalgam dental fillings. **(c)** Severe motion artifact in a CT image of the brain, caused by movement of the head during the scan. Image **(a)** and **(b)** from [5], **(c)** from [14].

object. All the one-dimensional attenuation profiles from the different angles can be back projected to recreate the attenuation in each voxel of the irradiated volume, thus obtaining the information to display the image.

Sometimes, errors will occur during the image aquisition, causing artifacts in the obtained images. Artifacts can arise from many different reasons [5], and Figure 2.6 shows three types of artifacts caused by bodily structures with high attenuation, the presence of metal objects in the body, and movement of the patient during the scan. If the cause of

the artifact is known, the image can be corrected for these errors after the image data is aquired to restore its diagnostic value.

A type of artifact related to the voxel size of the aquired image, is the partial volume artifact. When imaging a volume containing sharply contrasting borders, the borders in the object will seldom align perfectly with the edges of the detector elements [5]. The attenuation of the corresponding voxel will be described by averaging the x-ray energy reaching the detector. This can make objects appear blurred, or make thin objects appear wider than they are [15]. Reducing the slice thickness of the obtained images will reduce partial volume artifacts.

2.3.1 Tube current modulation

As a means to optimize the patient dose in CT, automatic tube current modulation (ATCM) was introduced for clinical use in 1994, and is currently implemented in CT scanners from every major manufacturer [16]. ATCM automatically adjusts the tube current to compensate for different attenuation at different positions in the patient, aiming at maintaining a target image quality throughout a scan. It thus provides a more consistent image quality throughout a single scan, and also between scans of different patients.

The tube current can be modulated along the z-axis to account for changes in attenuation along the length of the patient. This modulation is called *longitudinal modulation* [16], and increases the dose to high-attenuating areas like the pelvis, while decreasing the dose in low-attenuating areas like the lungs. In addition to the longitudinal modulation, the tube current can be modulated as the tube rotates around the patient in the xy-plane, to account for the changes in attenuation between different irradiation angles. This modulation is called *angular modulation*, and is especially important in regions of the body that have a very elliptical cross section, like the shoulders and abdomen. The angular modulation will increase the dose along the x-axis where the diameter of the patient is larger, and decrease the dose along the y-axis where the diameter of the patient is smaller. Longitudinal and angular modulation are illustrated in Figure 2.7.

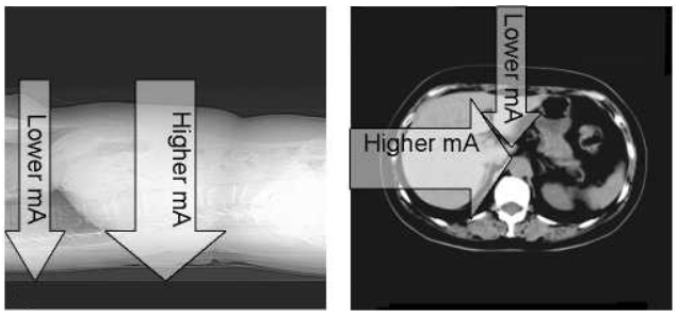

(a) Longitudinal modulation **(b)** Angular modulation

Figure 2.7: **(a)** Longitudinal modulation. Less mA is needed in the low-attenuating lung area than in the high-attenuating pelvis area. **(b)** Angular modulation. More mA is needed along the angles where the patient diameter is large, and less where the diameter is small. Images from [17].

The scanner estimates the attenuation of the patient based on one or two scanned projection radiographs (SPRs), where a projection image of the volume of interest is obtained with a fixed tube angle [16]. The attenuation data from the SPRs are then used to estimate the modulation needed along the scanned volume. Some scanners also utilize so-called *online modulation*, where data from the previous whole or half tube rotation is used to adjust the angular modulation during a scan.

Each vendor has based their ATCM system on one of two principles: image quality is evaluated either by a noise index, or by a dose index, i.e. a radiation dose estimated for a standard patient. A noise index is related to the standard deviation (SD) of pixel values in an image of a uniform phantom [16], and ATCM systems that use a noise index aims at keeping the image noise constant throughout a scan.

ATCM systems that use a dose index, are based on the hypothesis that different sized patients require different levels of image noise to obtain the desired diagnostic quality in an image [16]. Thus, they do not aim at keeping the image noise constant throughout a scan, and will allow more noise in images of thicker patients than they do for thinner patients.

An overview of the ATCM systems used on four different scanners are shown in Table 2.2.

Table 2.2: Overview of the ATCM systems used on four CT scanners.

Scanner	ATCM system	ATCM index	SPRs used
GE Revolution	Smart mA	NI	1
Philips Ingenuity	DoseRight	DRI	1
Siemens Somatom Definition Flash	CARE Dose4D	QRM	1
Toshiba Aquilion Prime	SureExposure	SD	2

ATCM, automatic tube current modulation; SPR, scanned projection radiograph; NI, noise index; DRI, dose right index; QRM, quality reference mAs; SD, standard deviation.

General Electric: Smart mA

General Electric's (GE) ATCM system is called Smart mA, and aims at maintaining a constant operator-selected noise level in the obtained images, independent of patient size and anatomy [18]. Each protocol has a reference noise index, NI, which can be adjusted up or down as needed by the so-called *Dose Steps*. Each step of increase of the Dose Steps will decrease the noise by 5%.

The tube current needed to obtain the desired image quality is determined by an anterior-posterior or lateral SPR, called a Scout. A second scout with a perpendicular projection is then estimated using a mathematical formula. The Smart mA system determines the tube current to be used based on the attenuation data from these two scouts.

Philips: DoseRight

In Philips' DoseRight system the operator provides the weight of the patient, which is used to estimate the a so-called *reference diameter* for the patient. For an adult with a weight of 50-90 kg, the body reference diameter is 29 cm. An SPR, called a Surview in the Philips' system, is obtained and the data used to calculate the diameter of the patient.

The deviations between the calculated diameter and the reference diameter are used to adjust the mAs given throughout the scan.

The desired image quality can be adjusted by the DoseRight Index (DRI), a discrete parameter designed to provide a consistent image quality for all patient sizes. At 120 kV, a DRI of 24 will give 200 mAs to a patient with a diameter of 29 cm. An increase in the DRI of +1 will result in a 12% increase in mAs, and a 6% decrease in noise [19].

Siemens: CARE Dose4D

Siemens' ATCM system is called CARE Dose4D, and uses a parameter called the *quality reference mAs* (QRM) to determine the desired image quality. The QRM is set equal to the effective mAs, i.e. mAs divided by pitch, that would be needed to obtain the desired image quality in a scan of a standard-sized patient (a 75 kg adult, or a 20 kg child) [20].

When using CARE Dose4D, an SPR is first obtained to measure the attenuation for one projection. The SPR is called a Topogram, and is obtained either for a posterior-anterior or lateral projection. A second topogram with a perpendicular projection is then estimated using a mathematical formula that takes the patient dimensions and anatomical region of interest into account. By using these two topograms, the optimal tube current for each angular projection can be estimated by the system, according to the QRM given as input by the operator. During the scan, online modulation is applied to fine tune the estimated optimal values. The adjustments are made based on the attenuation measured 180° earlier in the tube rotation.

Toshiba: SureExposure

With Toshiba's SureExposure system, one or two SPRs, called Scanograms, are obtained to allow for longitudinal or 3D (longitudinal and angular) modulation respectively [21]. From the scanograms the patient dimensions are converted to a "water equivalent diameter", which are used to adjust the tube current to match the image quality level specified by the operator. The image quality level is defined as a noise index, i.e. a target SD of noise in the images. Three global image quality settings are available for different body regions: High Quality, Standard and Low Dose. The settings are specified for different scan regions, like head and body both for adult and pediatric scans. The target SD can be adjusted from the three global settings as needed, either for a protocol to be used on multiple patients, or for one scan of a single patient.

2.4 Image reconstruction

During a CT procedure a preselected volume of the patient's body is scanned, and the data can be reconstructed as cross-sectional images along a chosen plane direction. The reconstruction can be done along the coronal plane, which divides the body into front and back, the sagittal plane, which divides the body into left and right, or the axial plane, which divides the body into top and bottom. Reconstructions can also be done along user specified angles. Figure 2.8 shows an illustration of the anatomical planes, together with CT images reconstructed along each plane direction.

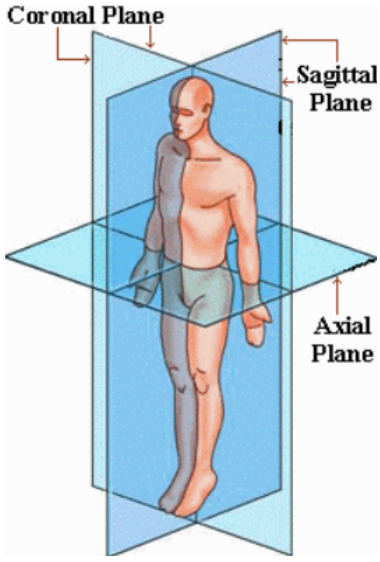

(a)

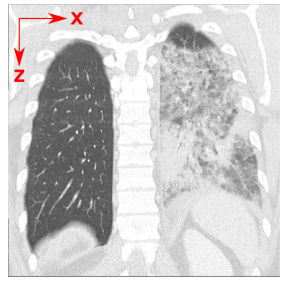

(b) Coronal

(c) Sagittal

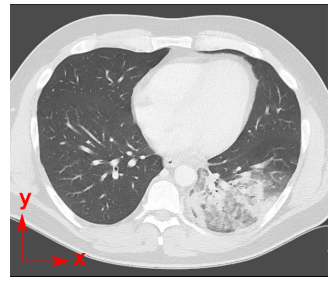

(d) Axial

Figure 2.8: **(a)** The anatomical planes, illustration from [22]. Reconstructions along the **(b)** coronal, **(c)** sagittal and **(d)** axial plane of CT images of a patient with legionnaires' disease. CT images from [23].

2.4.1 Image slice thickness

The choice of the aquired image slice thickness determines the depth of the image voxels, i.e. their length along the z-direction. A thick slice thickness will make each voxel cover a large area in the z-direction, and thus reduce the image resolution in the z-direction. It will also increase the chance of partial volume effects to occur (described in Section 2.3).

When using a thick slice thickness, the resolution in the images can be of good diagnostic quality along the axial plane, but become poor when the image data is reconstructed along the coronal or sagittal plane [24]. To ensure a similar image quality along any reconstructed plane direction, the image data should be obtained with isotropic, i.e. cubic, voxels, where the voxel depth is equal to the pixel size in the image.

While the voxel depth determines the thinnest reconstructed slice thickness available for the obtained image data, it is possible to reconstruct the images with a thicker slice thickness by combining data from several voxels. This will reduce the noise in the image by increasing the photon count in each voxel (see Section 2.6.2), and will also reduce the number of images for the radiologist to look through. This gives rise to the principle of "scan thin, view thick" [24], which calls for the image data to be obtained with a thin slice thickness, while the final images that are to be viewed by the radiologist are reconstructed in thicker slices.

2.4.2 Filtered back projection

The process of reconstructing a 2D image from the attenuation profiles in the sinogram is called *back projection* [9]. The intensities from each projection are summed to obtain the reconstructed image. A simple illustration of back projection is shown in Figure 2.9a.

To avoid signal intensity outside the actual object, a filter-function can be applied to the obtained attenuation profiles before a back projection is performed. This can reduce blurring and artifacts in the reconstructed image. The filter is applied by a mathematical convolution, and is illustrated in Figure 2.9b. This method is called *filtered back projection* (FBP).

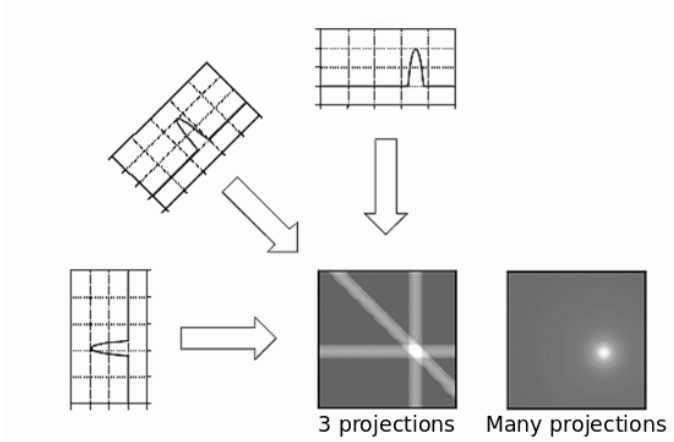

(a)

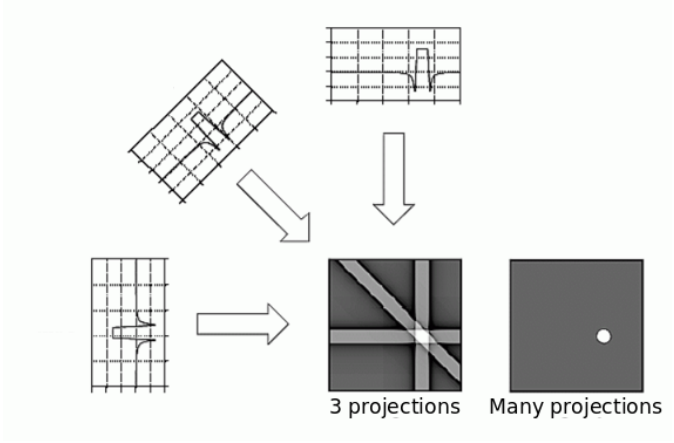

(b)

Figure 2.9: (a) Back projection and **(b)** filtered back projection (FBP) of an image using 3 and many projections. Illustrations from [25].

2.4.3 Iterative reconstruction

With FBP the measured raw data, i.e. the projection values, are used to create an image based on one single reconstruction. Another method, called iterative reconstruction (IR), use multiple repetitions of an iterative algorithm to converge the current solution (image) toward a better solution [26]. There are three major steps in IR. First, an estimated solution is forward projected to create artificial raw data. The process can be started with an empty image estimate, or by using prior information, e.g. an FBP reconstructed image estimate, if available. In the second step, the artificial raw data are compared with the real measured raw data, and a correction term is computed to account for the differences. In the third step, the correction term is back projected onto the current image estimate, to improve the current solution. The three-step IR-loop is repeated until a certain stop criterion is matched, which could be e.g. a certain number of iterations, that the correction term is small enough, or a specific quality criterion for the image is obtained. The IR process is illustrated in Figure 2.10.

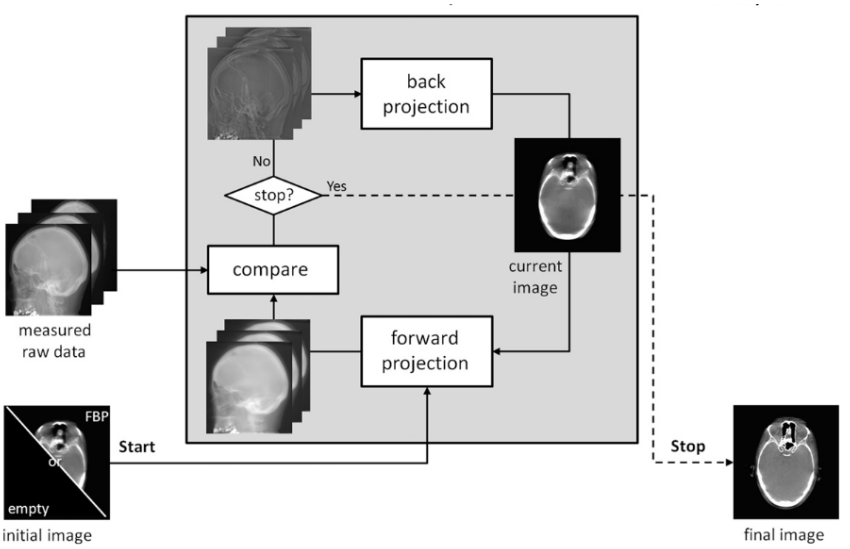

Figure 2.10: The process of iterative reconstruction (IR) is initiated with either an empty image estimate, or with prior information from e.g. an FBP reconstruction. A forward projection of the current image is used to create artificial raw data, which are compared to the real measured raw data. A correction term is calculated to account for the differences, and then back projected onto the current image to improve the current solution. The loop is terminated when a pre-defined stop criterion is fulfilled. Illustration from [26].

IR can give a more mathematically correct image reconstruction than FBP, and studies like Löve *et al* [27] have shown that the use of IR can reduce the noise in an image. It is thus often utilized as a means to reduce image noise without increasing the dose to the patient. In addition to reducing the noise IR will often affect the noise structure in an image, making the image noise appear as coarser grains compared to FBP reconstruction [27]. This will change how the image appears to an observer, and is often not desireable

for clinical purposes. The operator can specify the strength of the IR algorithm applied to the images, to balance the noise reduction benefit against an unwanted change in image appearance.

The IR solutions developed and implemented in modern CT scanners differ between vendors. An overview of the IR algorithms available from some vendors are listed in Table 2.3, together with the strength levels available for the operator to adjust the strength of the applied algorithm.

Table 2.3: IR algorithms from four CT vendors.

Vendor	IR algorithm	Strength levels
GE Healthcare	ASIR-V	0-100%
Philips Medical Systems	iDose	1-7
Siemens Healthcare	ADMIRE	1-5
Toshiba Medical Systems	AIDR 3D	Mild, Standard, Strong

IR, iterative reconstruction; ASIR-V, Adaptive Statistical Iterative Reconstruction - Veo; ADMIRE, Advanced Modeled Iterative Reconstruction; AIDR 3D, Adaptive Iterative Dose Reduction 3D.

2.5 Image display

The attenuation coefficient μ of an area in the body will vary with the x-ray energy of the incoming radiation beam [15]. To reduce each pixel value's dependence on the energy of the beam, a CT number is defined for each pixel relative to the attenuation coefficient of water, following the formula

$$CT_0 = 1000 \cdot \frac{\mu_0 - \mu_{H_2O}}{\mu_{H_2O}}. \tag{2.2}$$

Here, CT_0 is the CT number of the pixel expressed in Hounsfield units (HU), and μ_0 is the linear attenuation coefficient of the tissue in each pixel. This makes the pixel values dimensionless. The CT-numbers in an image will range from approximately -1000 for air, and up to 3000 for very dense bone. Water has a CT number of 0. Some CT numbers for different tissues and organs are listed in Table 2.4.

The CT numbers in an image are used to set the gray level of the displayed image, mapping each pixel value to one specific shade of gray [15]. By manipulating the mapping process, it is possible to change the appearance of the image to highlight a structure of interest without changing the actual pixel values. The gray levels are changed by changing the window width (WW) and window level (WL) of the image [28].

The WW determines the range of CT numbers that are displayed in the image. With a WW of 1000 HU, the available shades of gray will span over a range of 1000 HU, with all pixel values below the chosen range set to black, and all pixel values above set to white. A wide window will smooth out the transition from dark to light areas (i.e. between high- and low-attenuating materials), but will also make it hard to distinguish tissues with similar attenuation.

Table 2.4: CT numbers of different tissues at 120 kVp. Data from [15].

Tissue	CT number (HU)
Bone	1000-3000
Liver	50-80
Muscle	44-59
Blood	42-58
Water	0
Fat	-20 to -100
Lung	-300
Air	-1000

The WL determines the midpoint of the range of displayed CT numbers, and thus the brightness of the image. Increasing the WL of an image will make it appear darker, since more pixel values will fall below the chosen WW range. Similarly, decreasing the WL will make the image appear brighter. Some typical values for WW and WL are shown in Table 2.5, and a CT image displayed with three different windows is shown in Figure 2.11.

Table 2.5: Example of typical values for window width (WW) and window level (WL) for different structures of interest. The recommended values can vary somewhat between institutions and vendors. Data from [28].

Structure of interest	WW (HU)	WL (HU)
Brain	80	40
Liver	150	30
Abdomen soft tissues	400	50
Lungs	1500	-600
Bone	1800	400

(a) WW: 1800, WL: 400. **(b)** WW: 400, WL: 50. **(c)** WW: 1500, WL: -600.

Figure 2.11: One CT image of the heart and lung area of an anthropomorphic phantom, displayed with a **(a)** bone window, **(b)** abdomen soft tissue window and **(c)** lung window from Table 2.5. The appearance of each structure changes with different WW and WL.

2.6 Image quality

2.6.1 Spatial resolution

The spatial resolution of an imaging system is defined as its ability to differentiate two objects lying close together [9]. The spatial resolution can be described both in the spatial domain, i.e. by the smallest distance between two features that can be resolved individually, or in the spatial frequency domain, i.e. the highest spatial frequency that can be resolved by the system. Spatial frequency can be described as the number of line pairs present per centimeter (lp/cm), and the spatial frequency will increase as the lines move closer together. Figure 2.12 shows a CT image of a Catphan phantom module designed to test the spatial resolution of an imaging system. The lines move closer together for increasing spatial frequencies, requiring a better spatial resolution to be able to resolve the individual lines.

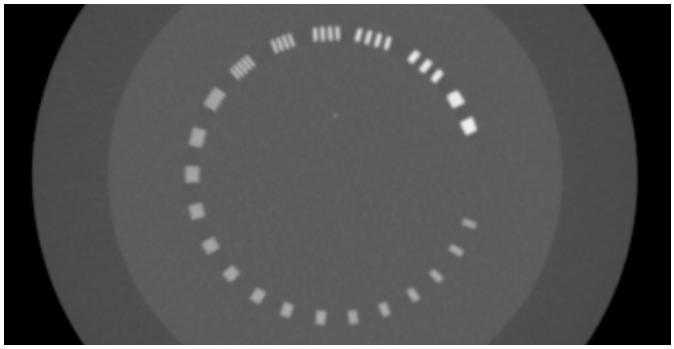

Figure 2.12: CT image of a Catphan CTP528 High Resolution Module, designed to test the spatial resolution of an imaging system. The image shows 21 groups of lines with spatial frequencies increasing counterclockwise from 1 to 21 lp/cm [29], i.e. an increase of 1 lp/cm per group of lines. In this image, the spatial resolution is approximately 6 lp/cm.

The spatial resolution will improve if an image consists of small pixels, since it allows for the visualization of variations over shorter distances in the imaged volume [15]. Thus, a slice thickness reduction along the axial plane will improve the spatial resolution in the z-direction.

2.6.2 Image noise

Noise in an image appears as unwanted fluctuations in its pixel values, i.e. the displayed gray levels. Noise can originate from all levels of the imaging chain, e.g. from optical imperfections, sampling or the digitization process.

In CT the main cause of noise is quantum noise, which results from the statistical nature of x-ray emissions [15]. The quantum noise can be reduced by increasing the statistical accuracy of the detected photons, i.e. increase the number of emitted, and thus detected, photons. Increasing the number of emitted photons will also increase the amount

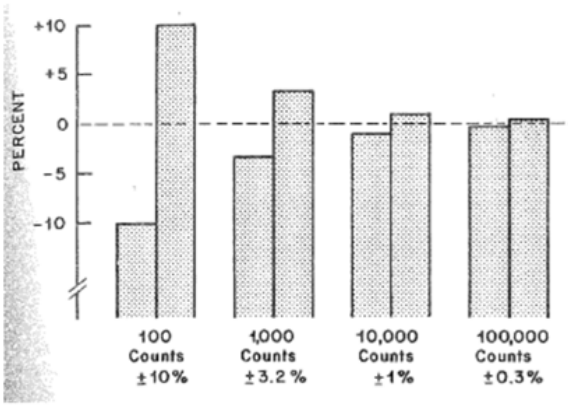

(a)

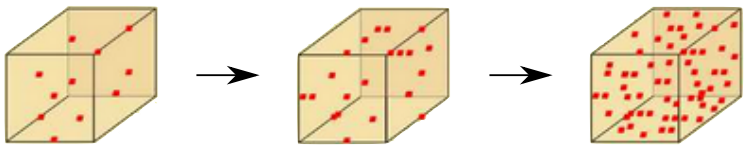

(b)

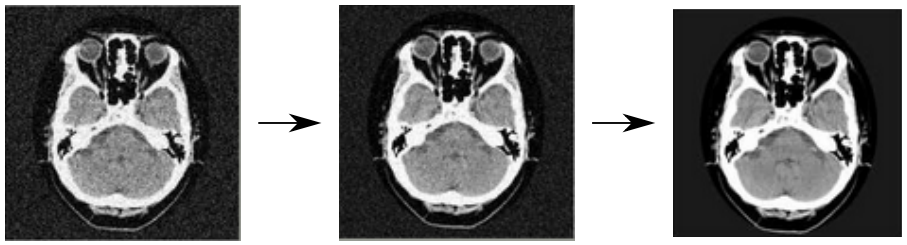

(c)

Figure 2.13: **(a)** Increasing the number of photons reaching the detector, i.e. the photon count, will decrease the statistical fluctuations in the number of detected photons. **(b)** Increasing the photon count will increase the amount of photons absorbed per voxel, which again will increases the probability for a voxel to display the correct HU value. **(c)** Increasing the amount of photons absorbed per voxel will decrease the image noise. Image **(a)** from [30], **(b)** and **(c)** from [31].

of photons absorbed per voxel, which will reduce the image noise. This is illustrated in Figure 2.13.

More photons will be emitted as the tube current is increased, and this will reduce the image noise as $1/\sqrt{\text{dose}}$ (see Figure 2.14). A noise reduction thus becomes a trade-off for increased image quality at the expense of increased dose to the patient.

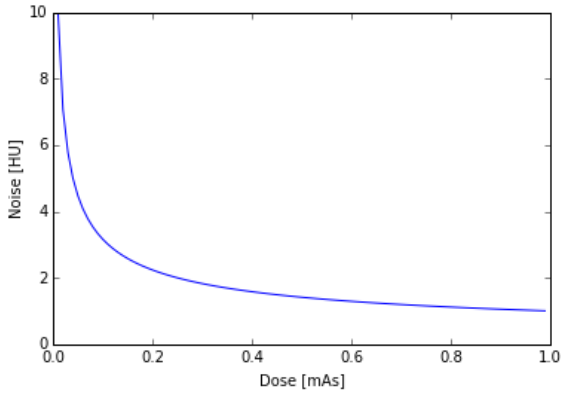

Figure 2.14: Noise in a CT image is reduced as the inverse square root of the dose .

Since image noise depends on the photon count inside a voxel, it will also be dependent on the size of the voxel. A larger voxel will receive a greater photon count for the same beam intensity compared with a smaller voxel. By reducing the CT image slice thickness, the volume of each voxel will decrease, thus creating more image noise for the same dose. The relationship between dose, noise and image slice thickness is explored further in Section 2.7

Noise is often measured as the standard deviation (SD) of the Hounsfield units in a defined region of interest (ROI) in a uniform area of the image. This value is easy to measure, but does not give any information about the structure of the noise, i.e. how the noise appears to an observer [32]. The same SD can appear very different depending on the spatial frequency of variations in the pixel values, as can be seen in Figure 2.15a.

Another method for measuring image noise that takes the noise structure into account, is the noise power spectrum (NPS). The NPS does not only take into account the variations in the pixel values in an ROI, but also the spatial frequency, i.e. the appearance, of these variations. An example of two NPS curves is shown in Figure 2.15b. A curve shifted to the left indicates low-frequency noise, which makes the noise appear as coarse grains in the image. A right-shifted curve, and thus high-frequency noise, indicates that the noise appears as finer grains.

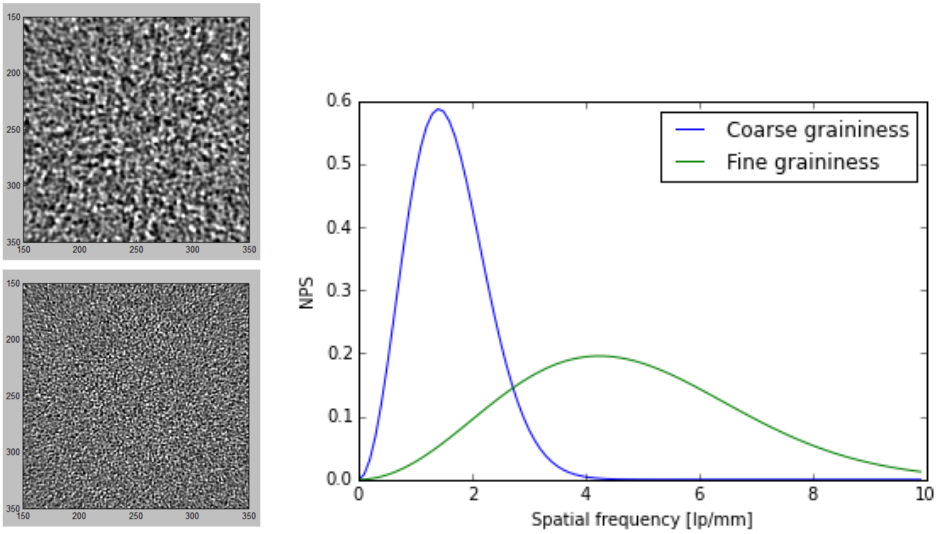

(a) **(b)**

Figure 2.15: (a) Two images with a pixel standard deviation of 21.5 HU. The noise appears different, with a more coarsely grained structure for the top image, and finer grains in the bottom image. Images from [32]. **(b)** Two NPS curves representing different noise structures. The blue curve is shifted to the left, indicating a coarse graininess (like the top image of **(a)**), while the green curve is shifted to the right, indicating a finer graininess (like the bottom image of **(a)**).

2.7 Brooks' formula

Since radiation dose and image quality are closely linked together, it is possible to create models to predict their relationship. One of these models is Brooks' formula, which was published in 1976 [33]. Brooks' formula assumes FBP as reconstruction method, and describes how the dose to the patient is affected by changes in different scan parameters in the following way:

$$D \propto \frac{\mathrm{e}^{-\mu d}}{\sigma^2 \cdot a^2 \cdot b \cdot h} \tag{2.3}$$

Here, D is the patient dose, μ is the mean attenuation coefficient and d is the object diameter, σ is noise described as the SD of CT numbers in the image, a is the sample increment, b the sample width and h the slice thickness of the image. When we are only interested in the relationship between radiation dose, image noise and slice thickness, Brooks' formula can be reduced to

$$D \propto \frac{1}{\sigma^2 \cdot h}. \tag{2.4}$$

According to Brooks' formula, a reduction of image slice thickness h can cause an increase in both the dose D to the patient, and in the image noise σ.

When investigating the effects of a slice thickness reduction, two extreme applications of Brooks' formula can be used: letting either the dose to the patient or the image noise

compensate entirely for the change in slice thickness. In these scenarios, the one parameter of the two that is not changed, will be kept constant during the slice thickness reduction. Applying Equation (2.4) to these two extreme scenarios: if h is halved and σ is to be kept constant, D must increase by a factor of two. If, on the other hand, D is to be kept constant, σ will increase by a factor of $\sqrt{2}$. Similarly, a reduction in slice thickness from 5 mm to 3 mm, which is by a factor of $3/5 = 0.6$, will result in an increase in the dose to the patient by a factor of $5/3 \approx 1.7$ if the image noise is to be kept constant, or a noise increase by a factor of $\sqrt{5/3} \approx 1.3$ if the dose to patient is to be kept constant. This scenario is illustrated in Figure 2.16.

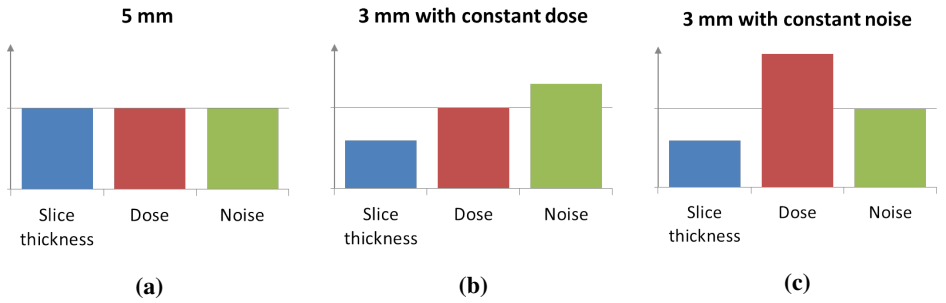

Figure 2.16: Illustration of the effects of a slice thickness reduction on both dose and noise, according to Brooks' formula (Equation (2.4)). **(a)** A protocol with a 5 mm slice thickness will result in a certain amount of dose being used, and a certain amount of noise in the obtained images. **(b)** If the slice thickness is reduced to 3 mm while the dose is kept constant, the image noise will increase by a factor of 1.3. **(c)** If the slice thickness is reduced to 3 mm and the image noise is to be kept constant, the radiation dose must increase by a factor of 1.7.

In clinical practice, a slice thickness reduction would be accounted for by some increase in dose, balanced against an acceptable increase in image noise.

2.8 CT dose descriptors

In traditional projection radiography, the patient is irradiated from a few angles. The dose is highest at the x-ray beam entrance, and decreases continually with penetration depth. This is illustrated in Figure 2.17a. In CT, the patient is irradiated from 360°, and the imaged volume is not irradiated simultaneously. This changes the dose distribution in the irradiated volume compared to projection radiography, as is illustrated in Figure 2.17b-c. This is one reason why it is not appropriate to use the same dose descriptors for CT as for conventional radiography [33].

The radiation dose output from the x-ray tube can be described by the tube current-time product (mAs), which is the product of the tube current and the tube rotation time. The dose imparted to a patient during a scan is often evaluated by two commonly used dose descriptors: the computed tomography dose index (CTDI) and the dose-length product (DLP). They both represent an estimated dose given to a standard CTDI-phantom. Both dose descriptors are estimated based on the chosen exposure parameters, and provided for

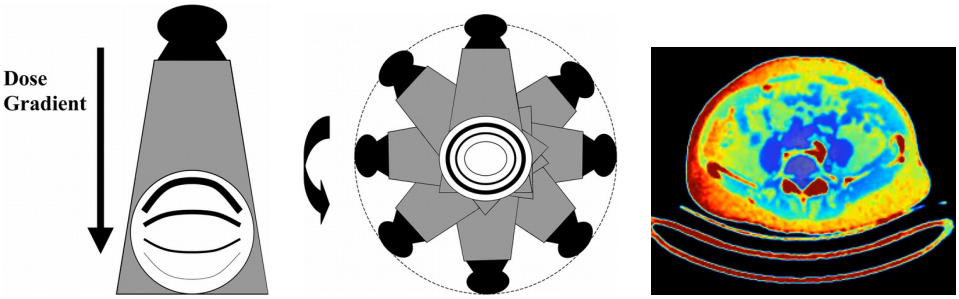

Figure 2.17: **(a)** In traditional projection radiography, the dose is highest at the beam entrance, as indicated by the thick curve, and decreases gradually towards the exit surface, indicated by the thinner curves. **(b)** In CT, the dose distribution is radially symmetric because of the 360°exposure, which is illustrated by the circular curves inside the irradiated object. The dose is highest at the surface, and decreases towards the center of the object. **(c)** A Monte Carlo simulation of the dose distribution at a given position and time in a helical CT scan. Red indicate high-dose areas, blue low-dose areas. Image **(a)** and **(b)** from [34], **(c)** from [35].

the operator prior to each patient scan. In this way, the operator can consider if any of the parameters should be changed to optimize the procedure.

2.8.1 Tube current-time product (mAs)

The tube current-time product (mAs) is proportional to the radiation dose to the patient. It can thus be used as an indicator of the dose imparted during a scan. This quantity takes into account the amount of photons created by the tube, and the amount of time the scanned object is exposed to this radiation.

The amount of received radiation for the scanned object will be dependent on other factors than just the mAs, like the distance from the tube to the table, so that an increase in mAs between two scans or scanners will not necessarily result in a similar increase in dose descriptors like CTDI and DLP. In addition to this, differences in components like the x-ray tube and the type of tube filtration used can affect the dose given per mAs, so that one scanner can impart a larger radiation dose for each mAs output from the tube.

2.8.2 Computed tomography dose index

The computed tomography dose index (CTDI) describes the dose imparted by a single rotation of the x-ray tube [33]. It is measured in the unit of milligray (mGy). Most of the dose will be deposited inside the radiation beam, but a part of it will also scatter outside of it. The CTDI sums up all the dose contribution along the z-axis for a single rotation, and represents the total imparted dose as if all dose was deposited inside the beam width. This is illustrated in Figure 2.18, for both one and multiple rotations. Mathematically, the CTDI can thus be described as

$$CTDI = \frac{1}{BW} \cdot \int_{-\infty}^{+\infty} D(z) \cdot dz \tag{2.5}$$

where $D(z)$ is the dose value at point z, and BW is the width of the radiation beam. The dose is often summed over a length of 100 mm, and the corresponding CTDI is called the CTDI_{100}.

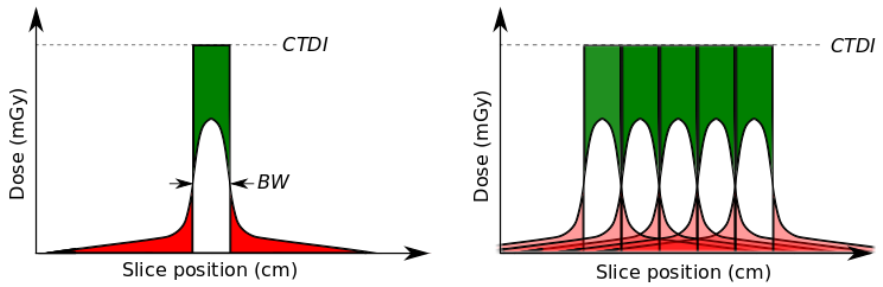

(a) One rotation **(b)** Multiple rotations

Figure 2.18: (a) The CTDI represents the total dose given in one rotation of the tube in a rectangular profile. The width of the profile is the beam width (BW), and the dose deposited outside the beam width is "moved" inside the beam (from the red area to the green area), determining the CTDI value. **(b)** For multiple rotations, the dose distribution is repeated with a shift in position for each rotation, here with $p = 1$. If we look at one fixed position, concidering both the dose imparted from the tube rotation around this position and the "tails" from the dose distributions from rotations on either side, the dose to one specific point will equal the CTDI.

The CTDI will depend on where in the beam the dose is measured. To account for differences in dose at different positions in the irradiated patient volume, a weighted CTDI, namely CTDI_w, is introduced. CTDI_w is obtained by measuring the CTDI in a so-called CTDI-phantom, illustrated in Figure 2.19. The CTDI is measured in five different points, one at the center and four at the periphery of the cylindrical phantom. The weighted dose index is obtained by the formula

$$CTDI_w = \frac{1}{3} CTDI_{center} + \frac{2}{3} CTDI_{periphery}, \tag{2.6}$$

where the $\text{CTDI}_{periphery}$ is the average dose value from the four periphery measurement points.

The dose imparted to a given volume will depend on the pitch of the scan, i.e. the overlap or distance between the radiation beam for each rotation. The volume CTDI, CTDI_{vol}, accounts for pitch related effects on the radiation dose:

$$CTDI_{vol} = \frac{CTDI_w}{p}. \tag{2.7}$$

CTDI_{vol} represents the average dose of a given scan volume, and is the dose quantity shown on the operator's console in all CT scanners [33].

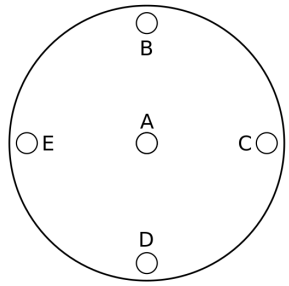

Figure 2.19: A CTDI-phantom, where CTDI_{center} is measured in position A, and $\text{CTDI}_{periphery}$ is the average of the measured CTDI in points B-E. The phantoms usually have a thickness of 15 cm in the z-direction, and a diameter of 16 or 32 cm to represent the size of a patient's head and body respectively.

2.8.3 Dose-length product

The dose-length product (DLP) is introduced as a means of comparing dose between scans of different lengths, and is the product of the radiation intensity (represented by CTDI_{vol}) and the scan length (L) [33]:

$$DLP = CTDI_{vol} \cdot L. \tag{2.8}$$

This gives it a unit of mGycm, and the DLP becomes a measure of the total dose imparted to the patient during the scan.

Chapter 3

Materials and methods

For this thesis, identical sets of measurements were performed on four newer CT models, one from each of the main CT vendors:

- GE Revolution (GE Healthcare, Waukesha, WI)
- Philips Ingenuity (Philips Healthcare, Cleveland, OH)
- Siemens Somatom Definition Flash (Siemens Healthcare, Forchheim, Germany)
- Toshiba Aquilion Prime (Toshiba Medical Systems, Otawara, Japan)

The scanners are located on three different radiological departments in Helse Vest: GE at Haraldsplass Diakonale sykehus (HDS), Philips at Kysthospitalet i Hagevik (KiH), and Siemens and Toshiba both at Haukeland University Hospital (HUS). All CT models have automatic tube current modulation (ATCM) and iterative reconstruction (IR).

A phantom was scanned with six different protocols on each of the four scanners. One scan was performed with each protocol on each of the four scanners, providing a total of 24 sets of images. The radiation dose and image noise was analyzed and compared between the different protocols and scanners.

3.1 ATCM phantom

The CCT228 ATCM phantom (The Phantom Laboratory, Greenwitch, NY) was developed by the CT physics group at the Karolinska University hospital in Stockholm, Sweden, and is meant to serve as a tool for characterizing the performance of different ATCM systems [36]. The phantom, shown in Figure 3.1, is made of a uniform material without any structures inside, making it well suited to investigate image noise and uniformity in addition to ATCM.

The phantom is divided into three elliptical sections of different dimensions to represent different bodily dimensions, all with a ratio of 3:2 between the diameter in the x- and

y-direction. The dimensions of each section are shown in Table 3.1. The shape of the phantom makes it possible to characterize both longitudinal (along the z-axis) and angular (in the xy-plane) ATCM: while the different sized sections demand tube current modulation in the z-direction, the elliptical cross section necessitates modulation in the xy-plane.

Because of time concerns and the quantity of obtained results, most of the image analysis was performed only on images from the large middle section of the phantom. It was decided to prioritize the analysis of images from this section because they displayed the most interesting behavior.

Figure 3.1: The ATCM phantom.

Table 3.1: Dimensions for each section of the ATCM phantom. D_x and D_y is the diameter in the x- and y-direction respectively, and L_z the length of each section in the z-direction.

	D_x [mm]	D_y [mm]	L_z [mm]
Small end section	250	167	150
Large middle section	350	233	150
Medium end section	300	200	150

3.2 Protocol specifications

One of the most commonly used protocols at HUS is the CT Thorax/Abdomen/Pelvis. One of the clinical indications for using this protocol is the follow-up of cancer patients, which necessitates a sufficient image quality for early detection of possible metastasis. At the same time, it is desirable to keep the radiation dose low, since the patient will need to perform the examination several times, normally every 3-6 months. The protocol covers a large volume of the patient's body, and uses dose modulation to adjust the dose and image quality throughout the scan. Also, this protocol has recently been revised by Helse Vest's standardization project. It was therefore decided to investigate the CT Thorax/Abdomen/Pelvis protocol in this thesis.

The American Association of Physicists in Medicine (AAPM) have published CT protocol recommendations for multiple scanners and procedures [3]. The protocols from AAPM serves as a neutral basis for radiologic procedures, unaffected by the preferences

of the local radiologists and radiographers in Helse Vest. AAPM recommend a slice thickness of 5 mm for their Thorax/Abdomen/Pelvis protocols, and was for this reason used as a basis when Helse Vest estimated the expected effects of a slice thickness reduction from 5 to 3 mm. It was therefore also chosen to use the AAPM protocol recommendations as a basis for the protocols used in this thesis, to serve as an objective standard for comparison of the protocol and scanner performances.

A set of six protocols were prepared, based on recommendations from AAPM for Thorax/Abdomen/Pelvis. These protocols were then used to scan the ATCM phantom on each of the four scanners. The protocols were adjusted to evaluate how a slice thickness reduction affects the automatic tube current modulation and image noise on each scanner, both when using FBP and IR algorithms as reconstruction methods.

3.2.1 Slice thickness reduction

To investigate how a reduction of slice thickness from 5 to 3 mm affects radiation dose and image noise, a protocol with a slice thickness of 5 mm was used as a starting point. This protocol was based on recommendations from AAPM for a Thorax/Abdomen/Pelvis scan [3]. The recommendations used for the CT scanners in this project are listed in detail in Appendix A. Through the rest of this thesis, the protocols with a slice thickness of 5 mm will be referred to as “5mm”.

Second, the slice thickness of the first protocol was reduced to 3 mm, while keeping the dose level constant from the 5mm protocol. This was done to evaluate the extreme case where the slice thickness reduction is accounted for in its entirety by a change in the image noise. The dose was kept constant by adjusting each vendors ATCM index (i.e. either a dose- or noise index) for all scanners by using Brooks’ formula in Equation (2.4). No other parameters were changed. This protocol is called “3 mm with constant dose”, or “3mm cD” for short.

Third, a second protocol with a slice thickness of 3 mm was used, where the image noise level was kept constant from the 5mm protocol. This was to investigate the extreme case where the slice thickness reduction is accounted for in its entirety by a change in the patient dose. The ATCM indices for each scanner was adjusted according to Brooks’ formula, and no other exposure parameters were changed. This protocol is called “3 mm with constant noise”, or “3mm cN” for short.

3.2.2 Image reconstruction

While Brooks’ formula is based on FBP reconstruction, all modern scanners also use IR as a reconstruction method. For this reason, it was decided to evaluate the image reconstruction algorithms used on the different scanners, by looking at the differences between using FBP and IR as image reconstruction methods. For this purpose, images obtained with the 5mm, 3mm cD and 3mm cN protocols were reconstructed in two different ways: with FBP, and with a medium level of IR, where the labels FBP and IR indicate the image reconstruction method used. Thus, scans with six different protocols were performed on each scanner:

- 5mm FBP
- 3mm cD FBP
- 3mm cN FBP
- 5mm IR
- 3mm cD IR
- 3mm cN IR

3.2.3 Protocol specifications for each scanner

Tables 3.2, 3.3, 3.4 and 3.5 show the protocol specifications used for the GE, Philips, Siemens and Toshiba scanner respectively. Each table shows the slice thickness[1], kV, rotation time, reconstruction kernel, IR level and the ATCM index used for each protocol.

The ATCM systems on the four CT scanners have implemented thresholds for the maximum and minimum tube current (mA) to be used during a scan. This is to keep the image quality from becoming unreasonably low, and keep the dose to the patient from becoming unreasonably high. Since the ATCM phantom differs from an actual patient and can be exposed to higher doses than a patient, these limits were not always suitable for our measurements. Since the dose modulation of the scanners were to be investigated, it was preferable that the curves showing the tube current-time product (mAs) would not be affected by the mA thresholds. In some scanners, the thresholds were easy to adjust up and down according to our needs. In other scanners, where the process of adjusting the mA thresholds were more complicated, it was decided because of time concerns to adjust the rotation time of the tube to keep the mA between the thresholds. By increasing the rotation time, the mA needed to obtain the desired image quality will be reduced, keeping it below the maximum mA threshold. Therefore, the rotation time for the 3mm cN FBP protocol on GE was increased from 500 ms to 1000 ms. Other than this specific case the rotation time was kept at 500 ms for all scanners, except for Philips, where the rotation time was adjusted automatically.

Table 3.2: GE Revolution protocol specifications.

Protocol	Thickness	kV	Rot. time	Kernel	ASIR-V	NI
5mm FBP	5 mm	120	500 ms	STANDARD	0 %	12
5mm IR	5 mm	120	500 ms	STANDARD	50 %	12
3mm cD FBP	2.5 mm[1]	120	500 ms	STANDARD	0 %	17
3mm cD IR	2.5 mm[1]	120	500 ms	STANDARD	50 %	17
3mm cN FBP	2.5 mm[1]	120	1000 ms	STANDARD	0 %	12
3mm cN IR	2.5 mm[1]	120	500 ms	STANDARD	50 %	12

ASIR-V, Adaptive Statistical Iterative Reconstruction - Veo; NI, noise index.

[1]Notice that the 3mm cD and 3mm cN protocols on GE actually have a slice thickness of 2.5 mm and not 3 mm. This was chosen due to inherent limitations in the choice of primary reconstruction slice thickness for the GE Revolution scanner, which among other things affected the readout of the mAs data in the images. The changes in GE's noise index between the protocols were adjusted accordingly, to account for a reduction in slice thickness from 5 to 2.5 mm instead of 3 mm.

Table 3.3: Philips Ingenuity protocol specifications.

Protocol	Thickness	kV	Rot. time	Kernel	iDose level	DRI
5mm FBP	5 mm	120	681 ms	B	-	24
5mm IR	5 mm	120	681 ms	B	3	24
3mm cD FBP	3 mm	120	679 ms	B	-	24
3mm cD IR	3 mm	120	679 ms	B	3	24
3mm cN FBP	3 mm	120	1012 ms	B	-	29
3mm cN IR	3 mm	120	1012 ms	B	3	29

DRI, dose right index.

Table 3.4: Siemens Somatom Definition Flash protocol specifications.

Protocol	Thickness	kV	Rot. time	Kernel	ADMIRE	QRM
5mm FBP	5 mm	120	500 ms	B30f	-	150
5mm IR	5 mm	120	500 ms	I30f	3	150
3mm cD FBP	3 mm	120	500 ms	B30f	-	150
3mm cD IR	3 mm	120	500 ms	I30f	3	150
3mm cN FBP	3 mm	120	500 ms	B30f	-	250
3mm cN IR	3 mm	120	500 ms	I30f	3	250

ADMIRE, Advanced Modeled Iterative Reconstruction; QRM, quality reference mAs.

Table 3.5: Toshiba Aquilion Prime protocol specifications.

Protocol	Thickness	kV	Rot. time	Kernel	AIDR 3D	SD
5mm FBP	5 mm	120	500 ms	FC18	ORG	12.5
5mm IR	5 mm	120	500 ms	FC18	STD	12.5
3mm cD FBP	3 mm	120	500 ms	FC18	ORG	16
3mm cD IR	3 mm	120	500 ms	FC18	STD	16
3mm cN FBP	3 mm	120	500 ms	FC18	ORG	12.5
3mm cN IR	3 mm	120	500 ms	FC18	STD	12.5

AIDR 3D, Adaptive Iterative Dose Reduction 3D; SD, standard deviation; ORG, original; STD, standard.

3.3 CTDI$_{vol}$

The CTDI$_{vol}$ is an indicator of the dose imparted by the x-ray tube to a standard CTDI phantom (as shown in Figure 2.19). After performing a CT scan a dose report is created, which shows both the average CTDI$_{vol}$ and DLP given by the tube during the scan. When comparing the imparted radiation dose between different scans, the DLP is often used since it takes into account both the CTDI$_{vol}$ and the scan length (see Equation (2.8)). The DLP can also be converted to an effective dose in millisievert (mSv) by using a conversion factor. For our scans, the scan length L will be identical for all scans, since the same phantom is used. For this reason, the CTDI$_{vol}$ is an equally suitable quantity to use for dose comparison as the DLP or effective dose.

For all protocols and scanners used in this project, the CTDI$_{vol}$ from all the dose reports were compared. The CTDI$_{vol}$ from the dose reports lies within an uncertainty interval of $\pm 10\%$ compared to measured values for all scanners used in this thesis (see Appendix E).

3.4 Tube current-time product (mAs) curves

All of the four scanners used in this project use automatic tube current modulation (ATCM), which adjusts the tube current according to the attenuation of the scanned object. Thus, a higher radiation dose will be given to high attenuating areas such as the pelvis or shoulders, and less dose to low attenuating areas such as the lung or neck. A mAs curve, which is a plot of mAs as a function of slice position, visualizes the tube current modulation. An example of a mAs curve showing the effect of ATCM on a scan of our phantom is shown in Figure 3.2.

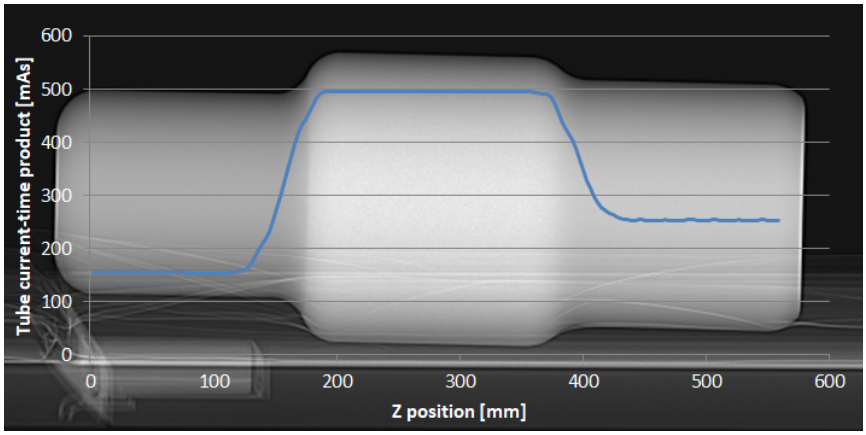

Figure 3.2: An example of a mAs curve obtained from a scan of the ATCM phantom. Automatic tube current modulation makes the mAs increase with the size of the phantom sections.

Throughout a scan, the mAs used at each slice position is saved in a so-called *digital imaging and communications in medicine* (DICOM) header for each image, together with

other relevant information about the image acquisition. The information stored in the DICOM header can be viewed by using e.g. a program called ImageJ [37]. By reading out the mAs from the DICOM header of each image for different image series, the mAs curves can be compared between different protocols and scanners. A Python script developed by physicist at Haukeland University Hospital, Daniel Aadnevik (and slightly modified by the author), was used to extract the mAs values from the image series in this thesis. The program code can be found in Appendix C.

3.5 Noise in the z-direction

Ideally for ATCM systems using a noise index, the noise level should be kept similar in all images throughout a scan regardless of changes in the attenuation of the object. With a phantom made of a uniform material, but with variations in diameter along the z-axis, it is easy to investigate if this is the case by calculating the SD noise in each image through a scan. This will reveal how the noise changes along the z-axis of the scanned object.

To calculate the SD noise in the obtained images, a program used to perform quality controls in medical imaging called ImageQC, developed by medical physicist at Stavanger University Hospital, Ellen Wasbø, was used [38]. A circular ROI with a radius of 70 mm was chosen, and this ROI was applied to the center of every image in each of the obtained image series. In this way, changes in SD noise along the z-axis can be compared between different protocols and scanners. The size and position of the applied ROI is visualized in Figure 3.3.

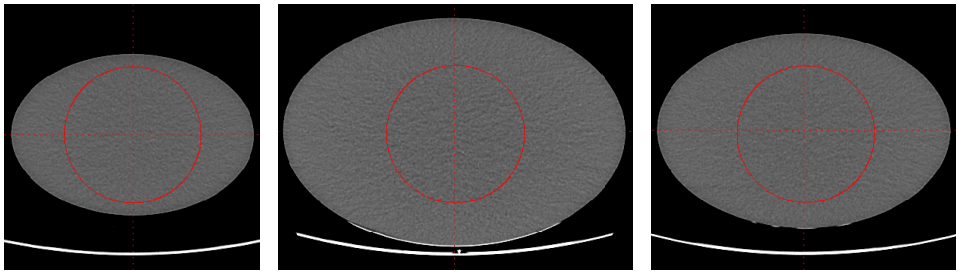

(a) **(b)** **(c)**

Figure 3.3: An ROI with a radius of 70 mm used for calculating the SD noise in the obtained images, visualized in the **(a)** small, **(b)** large and **(c)** medium sized section of the phantom.

3.6 Noise power spectrum

While noise as the SD in an ROI quantifies the variation of pixel values in a uniform area of an image, it does not give any information about the structure of the noise, i.e. the graininess of an image, or how the image noise is perceived by an observer. A noise power spectrum (NPS) on the other hand, is not only affected by the amount of noise present, but also by the noise structure: the amount of noise appears as the area under the NPS curve,

while the shape of the curve characterizes the noise structure, i.e. the image graininess. Since studies like Löve *et al* [27] have shown that the choice of reconstruction method can affect the noise distribution in an image, the NPS of each image series was calculated and compared between FBP and IR protocols. This was also done by using the program ImageQC.

To calculate the NPS for one image, 16 square ROIs, each with a size of 70 pixels, was distributed in a circle with a radius of 60 mm around the center of the phantom. This is illustrated in Figure 3.4. The sampling frequency was set to 0.010 mm^{-1}.

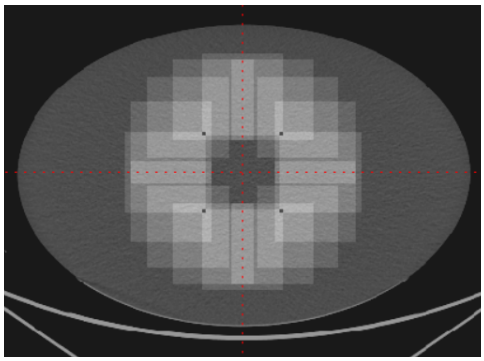

Figure 3.4: The ROIs used to calculate the NPS for an image is shown as light overlapping squares.

To calculate the NPS curve for an image series, all images covering the large middle section of the phantom was used. One NPS curve was calculated for each image, and the average NPS curve was calculated from all the individual curves. The number of images, and thus individual NPS curves used, varied from about 30 to 50 or 60, depending on the slice thickness of the protocol. To be able to quantify the shape of the NPS curves, their median values were calculated. The median value was chosen instead of the peak value, because the median accounts for the shape of the tail of the NPS curve.

3.7 Noise maps

A third noise measurement method, namely the creation of noise maps, can contribute with additional information about the spatial distribution of the noise in an image, i.e. how the noise varies between different parts of the image [39]. A noise map visualizes how each voxel in the imaged volume is affected by random noise fluctuations. This is done by comparing pixel values between a set of e.g. 50 identical images, instead of using pixel values in an ROI in one image. With a set of identical images where the size, structure and position of the imaged object does not change, the inter-image SD of the pixel values in one specific pixel location can be calculated, thus providing a measure of the impact of random noise fluctuations in this specific voxel. This process and an example of a resulting noise map is illustrated in Figure 3.5.

Since the phantom has similar attenuation characteristics and a uniform shape throughout each phantom section, the images from different slice positions in the same section will

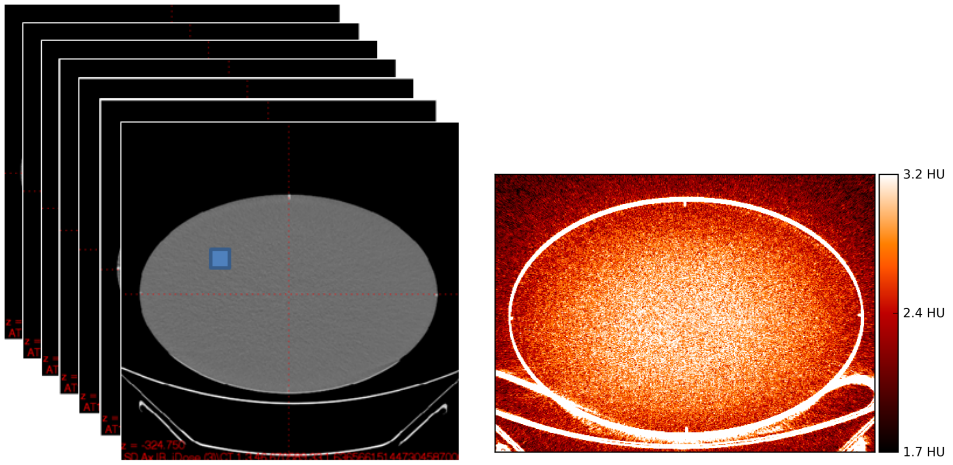

(a) **(b)**

Figure 3.5: **(a)** To create a noise map, the pixel values at a given pixel position, here illustrated in blue, is compared between a set of identical images. **(b)** The inter-image SD of the pixel values at each position in the images is mapped to a color scale, and becomes the pixel value at that same pixel position in the noise map.

maintain close to identical position, size and structure, so that a noise map can be created. To calculate noise maps for the image series obtained in this thesis, a Python script developed by physicist at Haukeland University Hospital, Helge Pettersen (and slightly modified by the author), was used. The program code can be found in Appendix D. One noise map was created for each protocol used on each scanner from the large middle section of the phantom, based on 30 or 50 images for 5 and 3 mm slice thickness respectively.

Chapter 4

Results

4.1 CTDI$_{vol}$

Figure 4.1a shows the change in CTDI$_{vol}$ when reducing the slice thickness from 5mm to 3mm cD. The 3mm cD protocols aim at keeping the dose constant compared to 5mm, and they show similar dose values as for 5mm on GE, Philips and Siemens.

Figure 4.1b shows the change in CTDI$_{vol}$ when reducing the slice thickness from 5mm to 3mm cN. The 3mm cN protocols aim at keeping the noise constant from 5mm, which would require an increase in dose. The GE, Philips and Siemens scanners all show an increase in dose between the 5mm and 3mm cN protocols.

The Toshiba scanner displays different behavior for the changes in CTDI$_{vol}$ compared to the other scanners, by showing a *decrease* in dose between 5mm and 3mm cD instead of keeping the dose constant. From 5mm to 3mm cN the dose values are similar, instead of showing an increase in dose. This behavoir is attributed to the fact that Toshiba always use a pre-defined slice thickness of 5 mm as a starting point when applying the chosen exposure parameters, regardless of the reconstructed slice thickness chosen by the operator. Because of this, similar and related tendencies are seen for all the following results obtained on Toshiba, both relating to radiation dose and image noise.

For Philips, Siemens and Toshiba the use of IR does not affect the CTDI$_{vol}$ compared to FBP. This is the case for 5mm, 3mm cD and 3mm cN. GE is the only scanner where the use of IR affects the CTDI$_{vol}$, and IR reduces the dose.

Table 4.1 shows the "coefficient of change" for CTDI$_{vol}$ when the slice thickness is reduced, i.e. the factor with which the CTDI$_{vol}$ changes between two protocols. The amount of change expected from Brooks' formula (Equation (2.4)) is also listed. The change is measured between 5mm and 3mm cD, and also for 5mm and 3mm cN. Changes are shown separately for FBP and IR. GE, Philips and Siemens all display small or no changes in CTDI$_{vol}$ for 5mm and 3mm cD. The three same scanners also show an increase similar to the expectations from Brooks' formula from 5mm to 3mm cN. Toshiba shows a decrease in dose (instead of similar values) from 5mm to 3mm cD, and similar values (instead of an increase) from 5mm to 3mm cN.

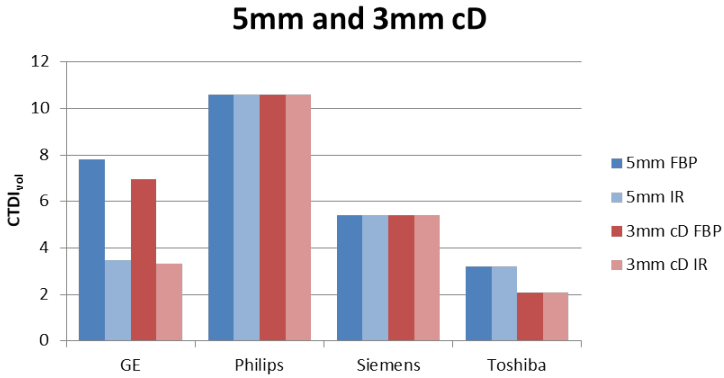

(a)

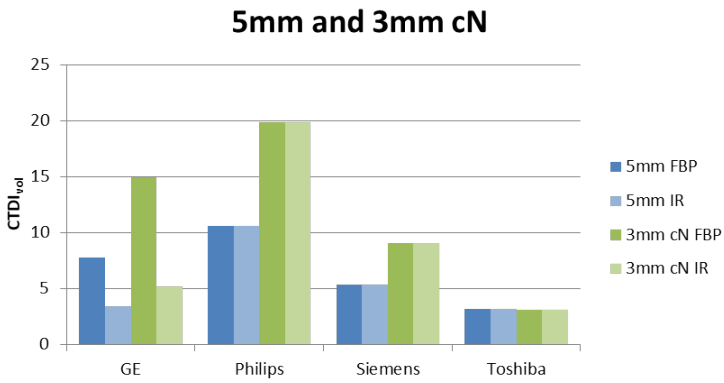

(b)

Figure 4.1: Average CTDI_{vol} for the **(a)** 5mm and 3mm cD protocols, and **(b)** 5mm and 3mm cN protocols for all scanners.

Table 4.1: Changes in the average CTDI_{vol} from the 5mm to the 3mm cD and 3mm cN protocols, together with the expected increase from Brooks' formula. The change is measured separately for FBP and IR protocols.

Change from: Change to:	5mm FBP 3mm cD FBP	5mm IR 3mm cD IR	5mm FBP 3mm cN FBP	5mm IR 3mm cN IR
GE	0.89	0.96	1.9*	1.5*
Philips	1.0	1.0	1.9	1.9
Siemens	1.0	1.0	1.7	1.7
Toshiba	0.66	0.66	0.97	0.97
Expected	1.0	1.0	1.7 (2.0)*	1.7 (2.0)*

*) The expected value listed in parenthesis is for the GE scanner

4.2 Tube current-time product (mAs) curves

The tube current-time product (mAs) at each slice position along the z-axis of the phantom is shown in Figures 4.2 and 4.3. Figure 4.2a-d presents mAs for the 5mm protocols together with the 3mm cD protocols, i.e. comparing the protocols where the dose was to be kept constant. Both Philips and Siemens have identical mAs curves for these two protocols, while GE and Toshiba shows a decrease in mAs for 3mm cD.

Figure 4.3a-d presents mAs for the 5mm protocols together with the 3mm cN protocols, i.e. comparing the protocols where the noise was to be kept constant. GE, Philips and Siemens show an increase in mAs for 3mm cN, while on Toshiba it is similar to 5mm.

GE is the only scanner where the mAs is affected by IR compared to FBP, and the use of IR reduces the mAs. For the other scanners, there was no change in mAs when using IR instead of FBP, and the curves for the corresponding protocols are overlapping.

Table 4.2 shows the amount of change in mAs from 5mm to the 3mm cD and 3mm cN protocols for the large middle section of the phantom. Changes when using FBP and IR are shown separately. The expected changes from Brooks' formula (Equation (2.4)) are also listed. Similar to the tendencies seen for the $CTDI_{vol}$, the GE, Philips and Siemens scanners all show an increase in mAs similar to what is expected from Brooks' formula. Toshiba on the other hand shows a decrease in mAs (instead of similar values) from 5mm to 3mm cD, and similar values (instead of an increase) from 5mm to 3mm cN.

Table 4.2: Changes in mAs in the large middle section of the phantom from the 5mm protocol to the 3mm cD and 3mm cN protocols, together with the expected increase from Brooks' formula. The change is measured separately for FBP and IR protocols.

Change from:	5mm FBP	5mm IR	5mm FBP	5mm IR
Change to:	3mm cD FBP	3mm cD IR	3mm cN FBP	3mm cN IR
GE	0.89	0.88	2.0*	2.0*
Philips	1.0	1.0	2.0	2.0
Siemens	1.0	1.0	1.7	1.7
Toshiba	0.74	0.74	1.0	1.0
Expected	1.0	1.0	1.7 (2.0)*	1.7 (2.0)*

*) The expected value listed in parenthesis is for the GE scanner

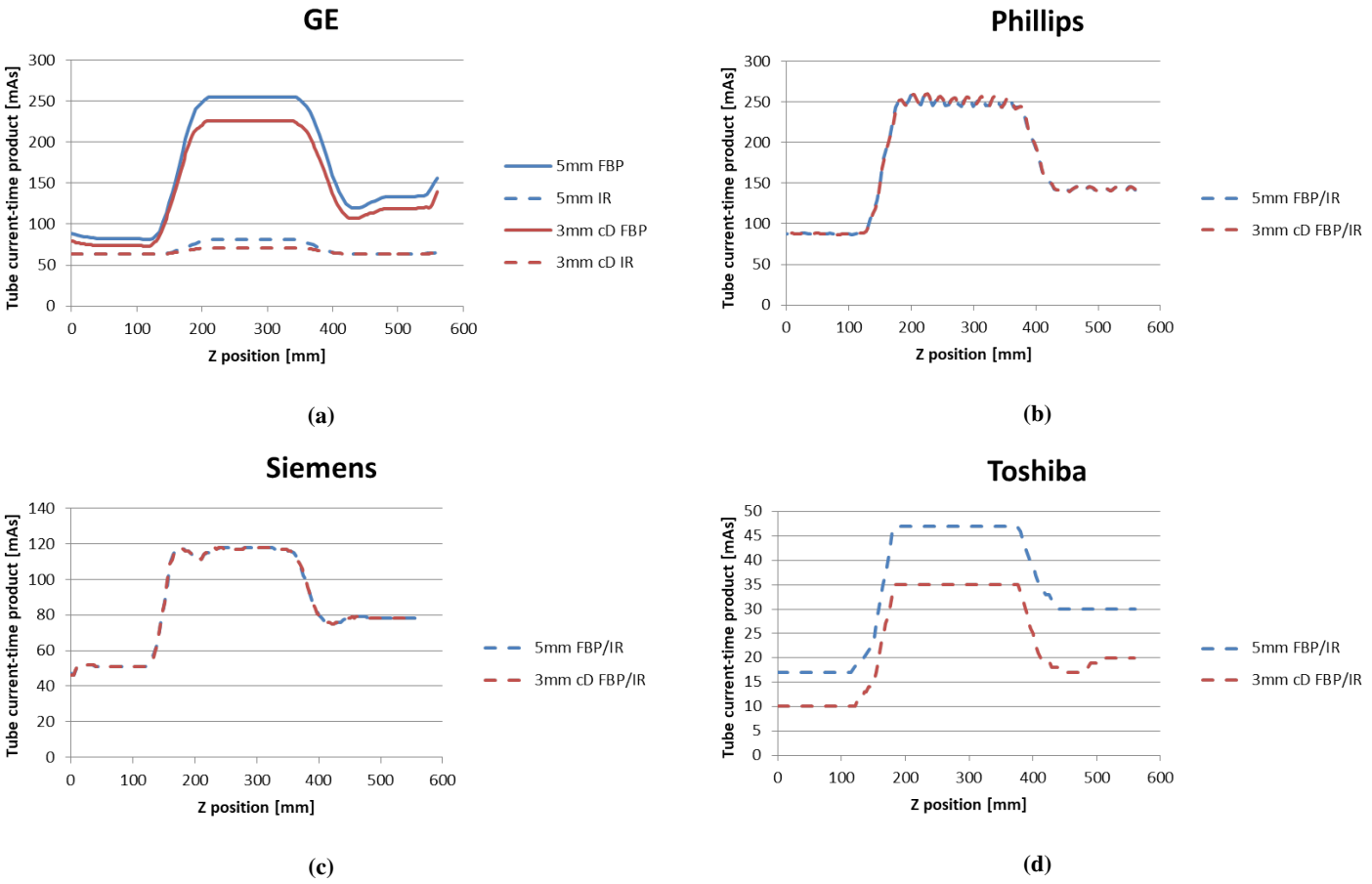

Figure 4.2: Tube current-time product in the z-direction for 5mm and 3mm cD protocols on the **(a)** GE, **(b)** Philips, **(c)** Siemens and **(d)** Toshiba scanner. For all scanners except GE the FBP protocols directly overlap their corresponding IR protocols, and the curve for FBP is omitted for clarity.

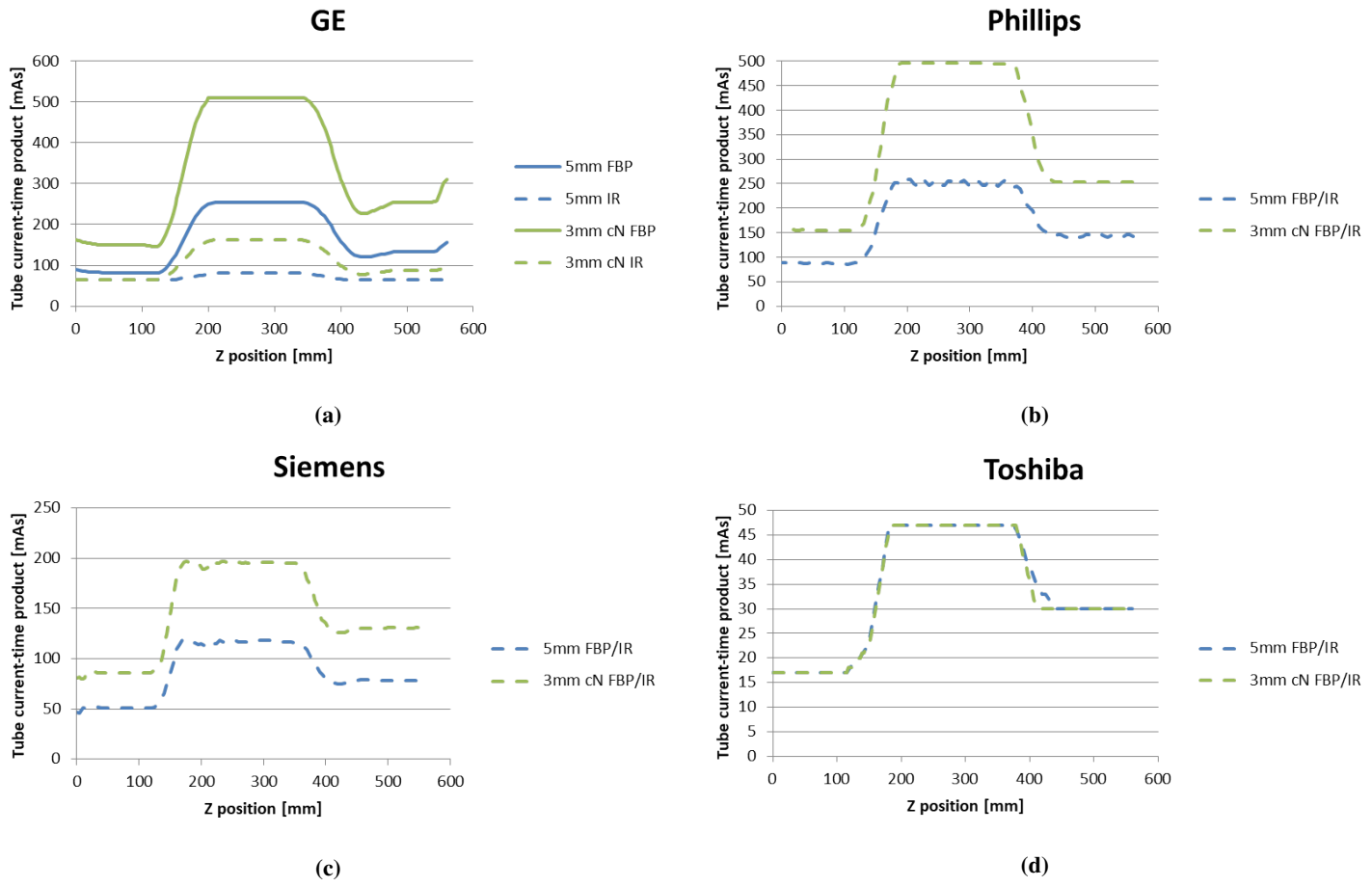

Figure 4.3: Tube current-time product in the z-direction for 5mm and 3mm cN protocols on the **(a)** GE, **(b)** Philips, **(c)** Siemens and **(d)** Toshiba scanner. For all scanners except GE the FBP protocols directly overlap their corresponding IR protocols, and the curve for FBP is omitted for clarity.

4.3 Noise in the z-direction

The noise as SD in an ROI along the z-direction of the phantom is shown in Figures 4.4 and 4.5. Figure 4.4a-d shows noise for the 5mm protocols together with the 3mm cD protocols, i.e. comparing the protocols where the dose was to be kept constant. All scanners show an increase in noise for 3mm cD.

Figure 4.5a-d shows noise for the 5mm protocols together with the 3mm cN protocols, i.e. comparing the protocols where the noise was to be kept constant. GE, Philips and Siemens show a similar noise level for 3mm cN compared to 5mm, while Toshiba shows an increase instead of similar values.

For Philips, Siemens and Toshiba the noise is reduced for all protocols when using IR compared to FBP. The same is not the case for GE, where FBP and IR show more similar noise levels in the large middle section of the phantom.

Table 4.3 shows the changes in noise in the large middle section of the phantom from 5mm to the 3mm cD and 3mm cN protocols. Changes when using FBP and IR are shown separately. The expected changes from Brooks' formula (Equation (2.4)) are also listed. Again, the changes for GE, Philips and Siemens follow Brooks' formula, while Toshiba shows a greater noise increase than the other scanners.

Table 4.3: Changes in noise in the large middle section of the phantom from the 5mm protocol to the 3mm cD and 3mm cN protocols, together with the expected increase from Brooks' formula. The increase is measured separately for FBP and IR.

Change from: Change to:	5mm FBP 3mm cD FBP	5mm IR 3mm cD IR	5mm FBP 3mm cN FBP	5mm IR 3mm cN IR
GE	1.5*	1.5*	1.1	1.1
Philips	1.3	1.3	0.91	0.92
Siemens	1.2	1.2	0.95	0.94
Toshiba	1.7	1.3	1.3	1.2
Expected	1.3 (1.4)*	1.3 (1.4)*	1.0	1.0

*) The expected value listed in parenthesis is for the GE scanner

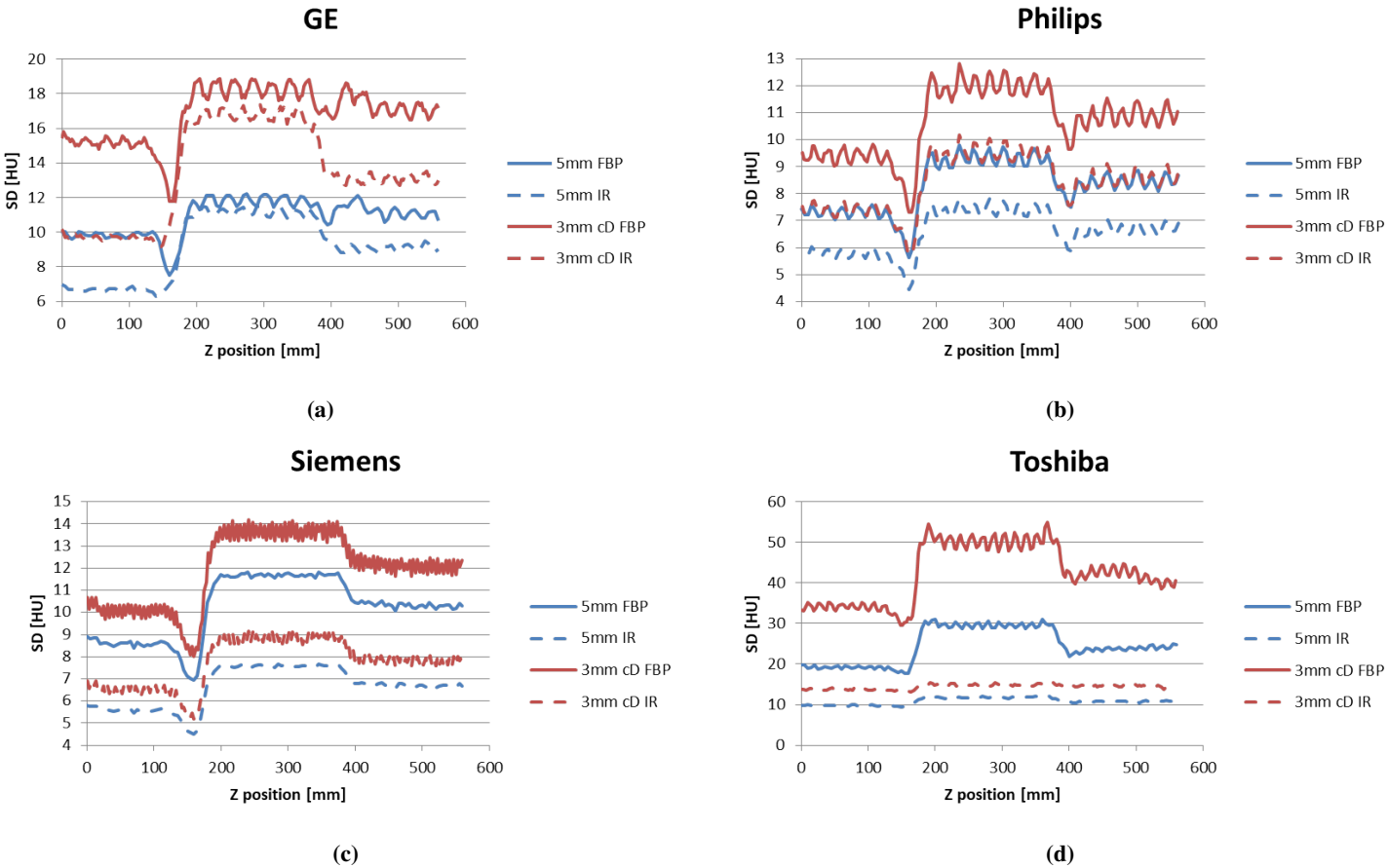

Figure 4.4: Noise along the z-direction for 5mm and 3mm cD protocols on the **(a)** GE, **(b)** Philips, **(c)** Siemens and **(d)** Toshiba scanner.

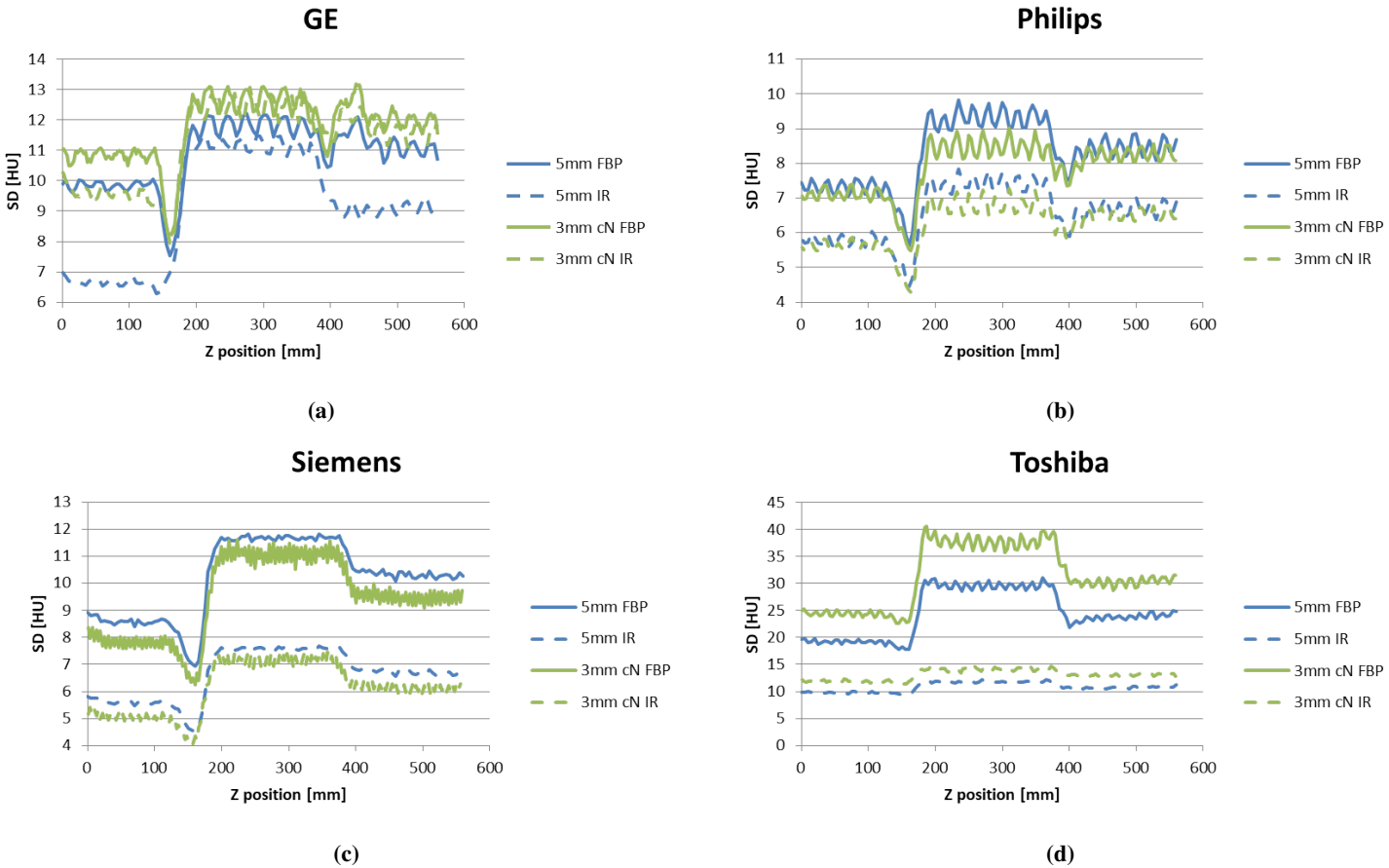

Figure 4.5: Noise along the z-direction for the 5mm and 3mm cN protocols on the **(a)** GE, **(b)** Philips, **(c)** Siemens and **(d)** Toshiba scanner.

4.4 Noise power spectrum

The median values for the NPS curves for all protocols and scanners are shown in Figure 4.6. The normalized NPS curves can be found in Appendix B. All scanners show a shift in median value towards the lower spatial frequencies for IR compared to FBP, indicating a change in the noise structure when using IR.

It is evident that the shift in median value from FBP to IR for a given protocol differ between the scanners. The average shift in median values between corresponding FBP and IR protocols on each scanner are listed in Table 4.4.

Table 4.4: Average shift in median values of the NPS curves for corresponding FBP and IR protocols on all scanners.

Scanner	Shift in median value
GE	29%
Philips	6%
Siemens	9%
Toshiba	40%

When looking at one single protocol group, e.g. 5mm, the median values can be sorted in ascending order:

- Toshiba IR
- GE IR
- Siemens IR
- Siemens FBP
- Philips IR
- Philips FBP
- GE FBP
- Toshiba FBP

This ascending order of median values is identical for 5mm, 3mm cD and 3mm cN, making the shift in median values similar between the different protocols.

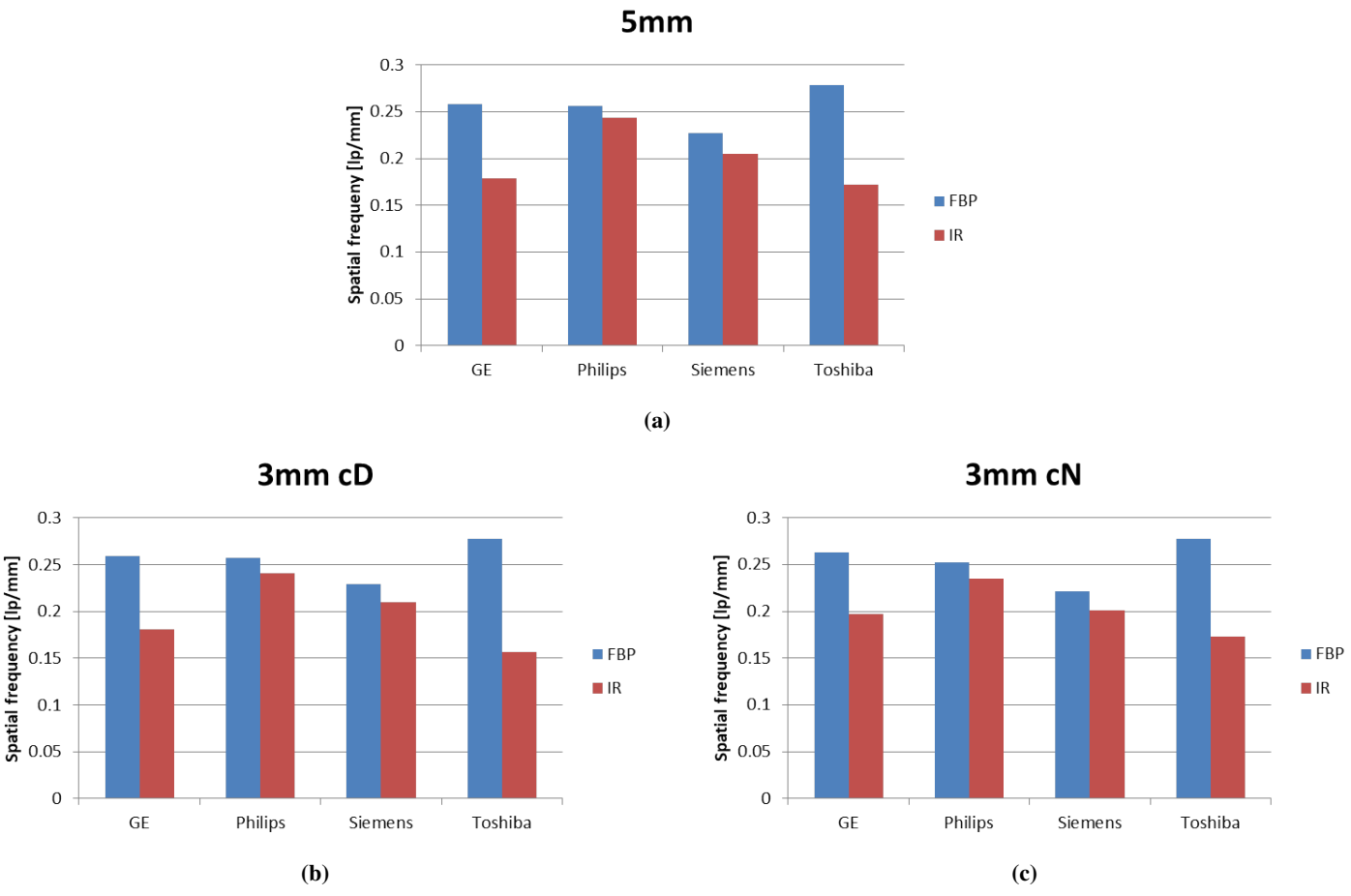

Figure 4.6: Median values for the NPS curves calculated for the **(a)** 5mm, **(b)** 3mm cD and **(c)** 3mm cN protocols on each scanner for FBP and IR.

4.5 Noise maps

Noise maps calculated from a set of images covering the large middle section of the phantom are shown in Figures 4.7, 4.8, 4.9 and 4.10 for the GE, Philips, Siemens and Toshiba scanner respectively. One map was created for each protocol used on each scanner.

The noise maps show the spatial distribution of the noise, and the color scale indicates the noise level in each set of images. The color scale is adjusted for each scanner to show clearly how the noise distribution changes for each protocol, and can thus not be compared between scanners.

GE, Philips and Siemens display similar spatial noise distributions, with more noise in the center of the phantom and less towards the phantom edges. This distribution is present for all protocols. As for Toshiba, with FBP the noise is distributed in a band through the thickest section of the elliptical phantom. When IR is used the band is replaced by a uniform noise distribution throughout the phantom.

As has already been demonstrated in Section 4.3, the noise level decreases from FBP to IR for Philips, Siemens and Toshiba, i.e. the shades of color in the noise map darkens. GE is again the exception to this, with a noise level that looks similar for both FBP and IR.

For GE, Philips and Siemens the noise level seems to be reduced with approximately the same amount each time IR is used, independent of the original noise level in the image. The protocols showing the highest and lowest noise level when reconstructed with FBP, are still showin the highest and lowest noise level respectively when reconstructed with IR. For Toshiba on the other hand, the correlation between the noise level in the FBP and IR maps is less obvious, and all of the IR maps have a more similar noise level than for any other scanner.

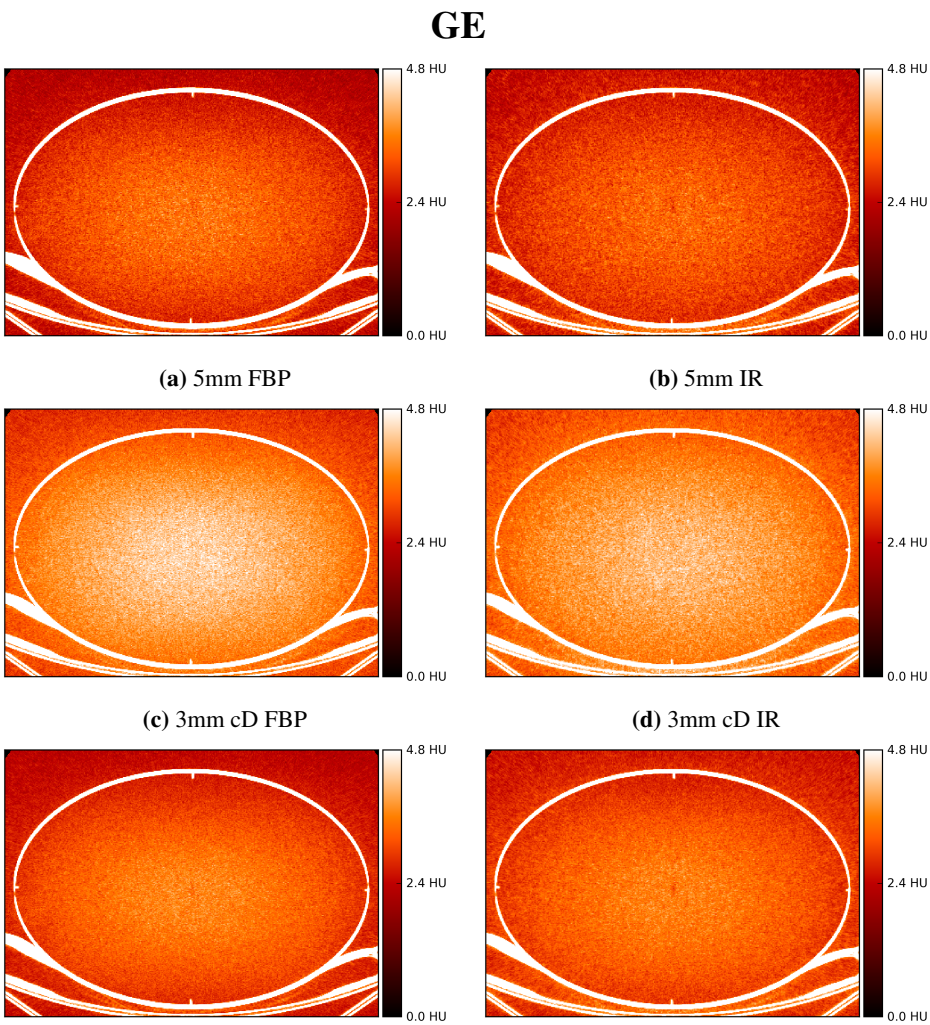

(a) 5mm FBP **(b)** 5mm IR

(c) 3mm cD FBP **(d)** 3mm cD IR

(e) 3mm cN FBP **(f)** 3mm cN IR

Figure 4.7: Noise maps for all protocols on the GE scanner.

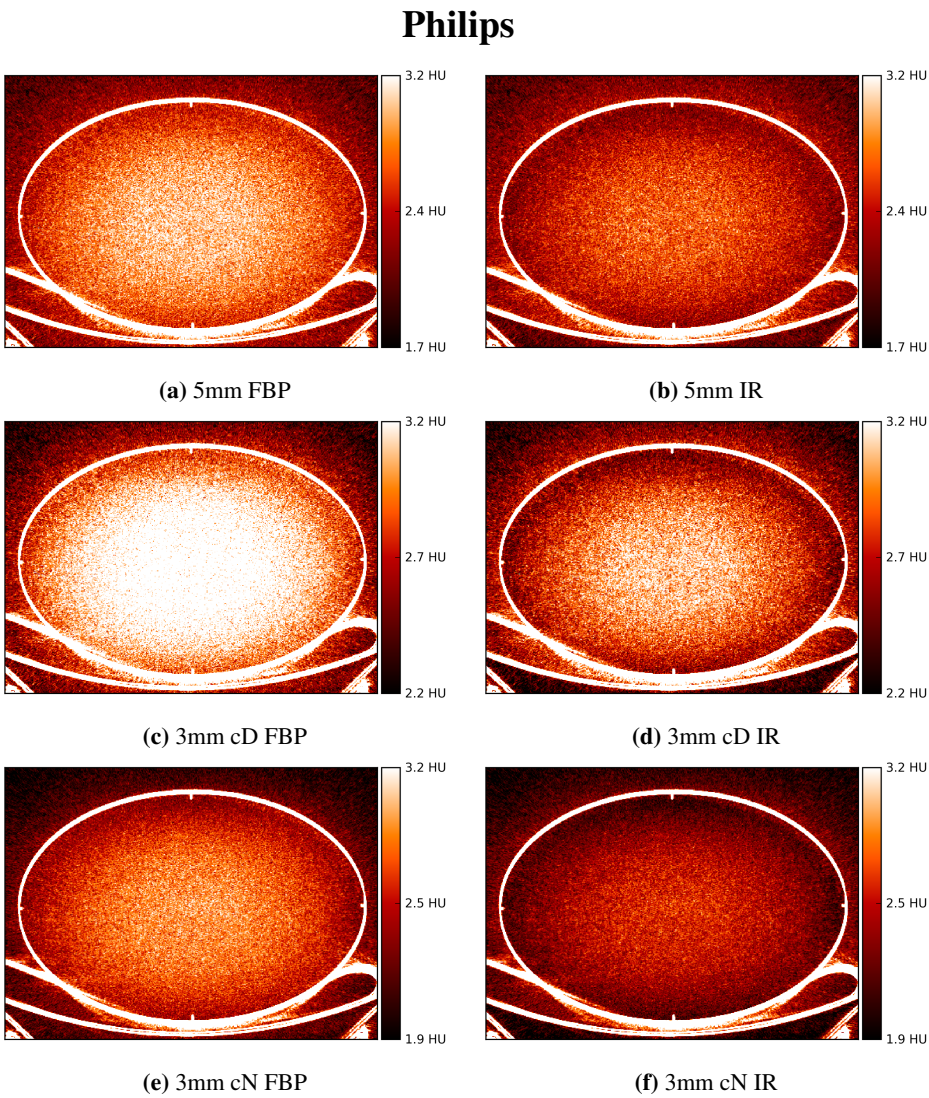

(a) 5mm FBP **(b)** 5mm IR

(c) 3mm cD FBP **(d)** 3mm cD IR

(e) 3mm cN FBP **(f)** 3mm cN IR

Figure 4.8: Noise maps for all protocols on the Philips scanner.

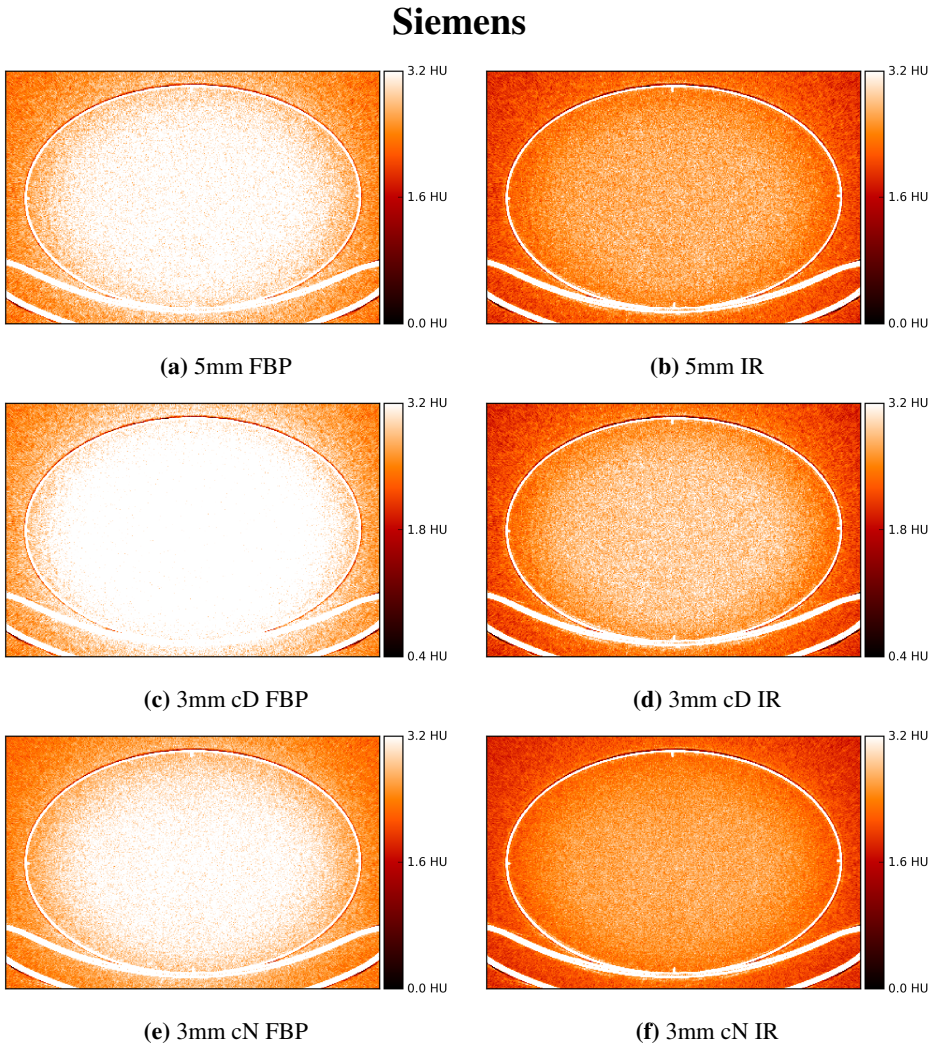

(a) 5mm FBP **(b)** 5mm IR

(c) 3mm cD FBP **(d)** 3mm cD IR

(e) 3mm cN FBP **(f)** 3mm cN IR

Figure 4.9: Noise maps for all protocols on the Siemens scanner.

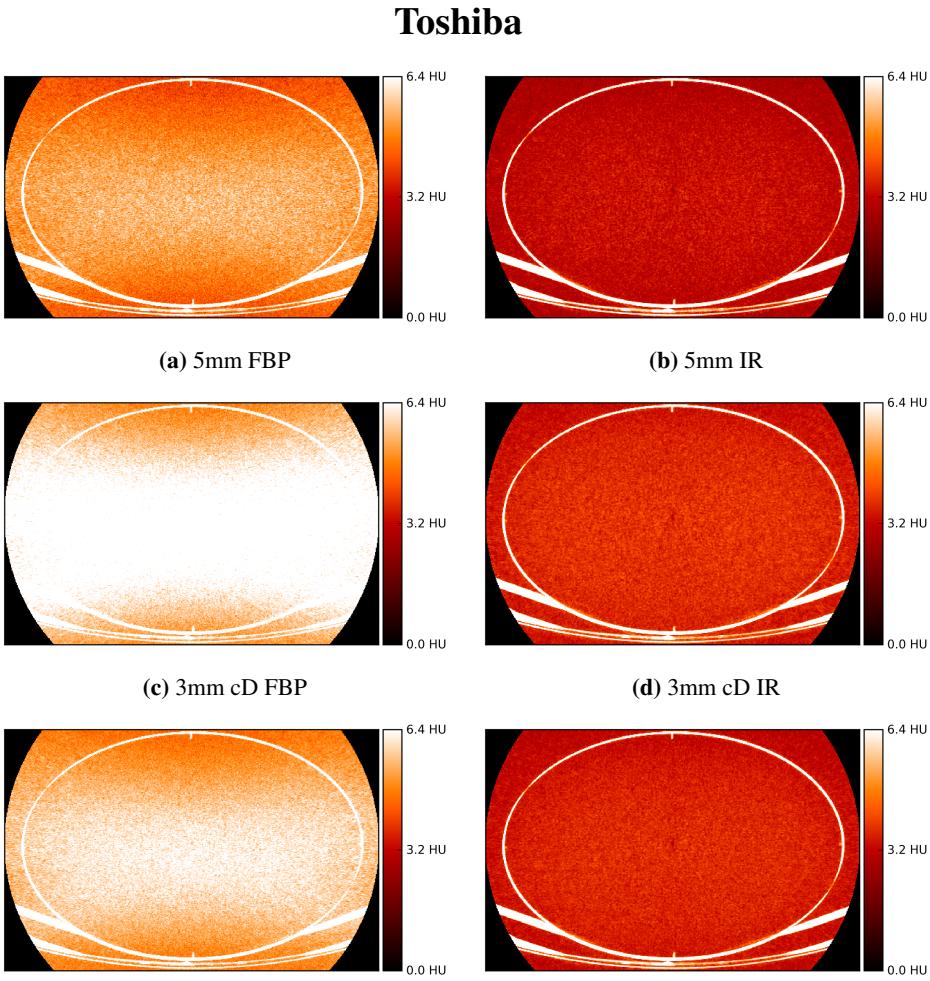

(a) 5mm FBP **(b)** 5mm IR

(c) 3mm cD FBP **(d)** 3mm cD IR

(e) 3mm cN FBP **(f)** 3mm cN IR

Figure 4.10: Noise maps for all protocols on the Toshiba scanner.

Chapter 5

Discussion

Different CT scanners work in slightly different ways, and when comparing their performance it is necessary to find an objective standard of comparison to use as a basis. Since the AAPM has published recommendations for protocol specifications to use for procedures performed on different scanners [3], their protocols presented a natural starting point for evaluating the effects of the slice thickness reduction that has been introduced in Helse Vest.

By letting the image slice thickness reduction be accounted for in its entirety either by an increase in radiation dose or an increase in image noise, the two most extreme effects that could occur from the slice thickness reduction could be evaluated. In a clinical setting, an increase in both radiation dose and image noise would be used to accound for the slice thickness reduction, and is thus expected to yield less change in both dose and noise compared to the results obtained in this thesis.

5.1 Brooks' formula

Despite being more than 40 years old and based on FBP reconstruction, Brooks' formula can still serve as a starting point when performing estimates of dose and noise behavior on modern CT scanners. This is evident from Tables 4.1, 4.2 and 4.3, where the dose and noise increase for GE, Philips and Siemens correspond well to the predictions from Brooks' formula. This is the case not only when using FBP, but also for IR.

At first glance, Tables 4.1-4.3 seem to suggest that Brooks' formula did not provide accurate predictions on the Toshiba scanner, but this is not the case. The differences in dose and noise behavior for Toshiba compared to the other scanners is a result of how the scanner applies the chosen input exposure parametres, which will be discussed in detail in Section 5.4. When this is accounted for, the changes in dose and noise for Toshiba was also in accordance with the expectations from Brooks' formula.

These results indicate that the estimates made by Helse Vest for the standardization projects using Brooks' formula are trustworthy.

5.2 3 mm with constant dose

The aim of the 3mm cD protocol was to keep the dose constant from the 5mm protocol, while accepting an increase in image noise.

Changes in dose level

For the GE scanner, the $CTDI_{vol}$ and mAs show similar values for the 5mm and 3mm cD protocols (see Tables 4.1-4.2). This is as expected from Brooks' formula.

For Philips and Siemens, the $CTDI_{vol}$ and mAs for 5mm and 3mm cD is not only similar, but identical. Both vendors have based their ATCM system on evaluating the image quality in terms of a dose index estimated to a standard patient, instead of using a noise index. When one scan was performed with the ATCM dose index recommended by AAPM, the same set of raw data could be reconstructed into several sets of images with a chosen slice thickness and reconstruction method. On the Philips and Siemens scanners, the four image series obtained with the protocols 5mm FBP, 5mm IR, 3mm cD FBP and 3mm cD IR all used the same dose index (see Tables 3.3 and 3.4), and they could thus be reconstructed from the same set of raw data. Because of this, the $CTDI_{vol}$ and mAs given for the four image series must necessarily be identical.

For the Toshiba scanner, the $CTDI_{vol}$ and mAs behaved differently compared to the other scanners. Instead of remaining at similar levels from 5mm to 3mm cD, they were both reduced. The reason for this is discussed in detail in Section 5.4

Changes in noise level

The changes in noise from 5mm to 3mm cD necessarily reflects the changes in dose described above. Just as GE, Philips and Siemens all displayed dose values as expected, they also showed an increase in image noise as expected: an increase close to 1.3 (1.4 for GE), similar to the expected values from Brook's formula for both FBP and IR protocols (see Table 4.3).

For Toshiba, the noise increased more than expected for the 3mm cD FBP protocol. This is in accordance with the decrease in $CTDI_{vol}$ and mAs described above, which would result in an increased amount of image noise. For the 3mm cD IR protocol on Toshiba, the noise increase is in accordance with the estimates made with Brooks' formula, indicating that the use of IR has reduced the noise more in the 3mm cD IR images than the 5mm IR images. This tendency for IR on Toshiba will be discussed further in Section 5.5.

5.3 3 mm with constant noise

The aim of the 3mm cN protocol was to keep the noise level constant from 5mm, thus necessitating an increase in dose.

Changes in dose level

For the GE, Philips and Siemens scanners the $CTDI_{vol}$ and mAs behaved as expected, with an increase in dose close to 1.7 (2.0 for GE). These tendencies were seen for both

FBP and IR protocols. This is similar to the predictions made by Brooks' formula (see Table 4.1-4.2).

For the Toshiba scanner, the CTDI_{vol} and mAs behaved differently compared to the other scanners. Instead of increasing the dose from 5mm to 3mm cN, they both remain at similar dose levels. The reason for this is discussed in detail in Section 5.4.

Changes in noise level

For GE, Philips and Siemens the noise level is similar between 5mm and 3mm cN (see Table 4.3). This was the case for both FBP and IR, and reflects the changes in dose level described above. This behavior is in accordance with the expectations from Brooks' formula.

Toshiba again shows different behavior compared to the other scanners, by showing an increase in noise (see Table 4.3). This noise increase corresponds with the lack of dose increase discussed above.

5.4 Differences in dose and noise behavior between scanners

The protocols on Toshiba did not follow Brooks' formula in the same way as the other scanners when trying to keep the dose and noise constant from the 5mm protocol (see Tables 4.1-4.3). This is assumed to be a result of how Toshiba interprets the exposure input parameters chosen by the operator.

When preparing a protocol on Toshiba, the scanner always uses a pre-defined slice thickness of 5 mm as a basis when applying the chosen SD noise index and other exposure parameters. This is the case also when the final image series is to have a reconstructed slice thickness of e.g. 3 mm.

When transitioning from the 5mm to the 3mm cD protocol, the Toshiba SD noise index was increased according to Brooks' formula to keep the dose constant, i.e. from SD $= 12.5$ to SD $= 16$ (see Table 3.5). The noise index of 16 was then applied by the scanner to a pre-defined slice thickness of 5 mm. In this way, the pre-defined 5 mm images obtained with the 3mm cD protocol will have a higher noise level than the pre-defined 5 mm images obtained with the 5mm protocol. This will result in a lower dose output from the scanner, explaining the decrease of both CTDI_{vol} and mAs from 5mm to 3mm cD. The reconstruction with the chosen slice thickness of 5 and 3 mm respectively, is performed after the image raw data is obtained, and thus after the chosen noise index has been applied to the pre-defined 5 mm slice thickness.

The pre-defined slice thickness of 5 mm is kept unchanged between the 5mm and 3mm cD protocol. According to Brooks' formula, if the slice thickness is kept constant while the noise index is increased from 12.5 to 16, the dose will change by a factor of 0.61, i.e. the dose will decrease. This decrease predicted by Brooks' formula is similar to the actual measured change in dose on Toshiba: a change of 0.66 for CTDI_{vol} and 0.74 for mAs (see Tables 4.1-4.2).

As for the 5mm to 3mm cN protocol transition, the same SD noise index was used for both protocols to keep the image noise constant. Thus, identical noise indices were

applied to the pre-defined slice thicknss of 5 mm, which would require the same dose. This is the reason for the similar $CTDI_{vol}$ and mAs values between these two protocols. Reconstructing the raw data into 3 mm thick images will increase the noise according to Brooks' formula, and the noise increase seen from 5mm to 3mm cN on Toshiba is therefore close to 1.3. This is similar to the noise increase seen for the 3mm cD protocols on the other scanners (see Table 4.3).

For all protocols, Toshiba used a lower mAs than the other scanners (see Figures 4.2-4.3). This is assumed to be a result of the differences in dose yield, i.e. the dose delivered per mAs, for the four scanners. Toshiba also use less filtration of the radiation beam, giving the scanner a softer x-ray spectrum compared to the other vendors. This will cause the beam to be more attenuated in the scanned object, resulting in more noise in the image compared to the other scanners, as seen in Figures 4.4-4.5.

5.5 Effects of iterative reconstruction

Dose- or noise reduction benefit

On the GE scanner, the noise in the large middle section of the phantom was similar for both FBP and IR protocols (see Figures 4.4-4.5). This is because the dose was reduced when using IR, as can be seen from the reduction of $CTDI_{vol}$ and mAs shown in Figures 4.1-4.3. The GE noise maps (Figure 4.7) also show similar noise levels between FBP and IR. This indicates that the GE scanner estimates the expected amount of noise reduction that will be performed by the IR algorithm, and reduces the dose accordingly. Using IR thus provides an added benefit with respect to dose reduction, and both the FBP and IR reconstructed images have similar levels of image noise (see Figure 4.4a and 4.5a). Similar results for GE have been shown by Merzan *et al* [16].

As for the Philips, Siemens and Toshiba scanners, the $CTDI_{vol}$ and mAs was not affected by the choice of image reconstruction method. This resulted in the noise decrease shown for the SD noise along the z-axis in Figures 4.4-4.5, and the decrease in noise level from the noise maps in Figures 4.8-4.10. The noise reduction performed by the IR algorithms on these scanners will thus provide an added benefit to the image quality, and not affect the radiation dose.

Shift in spatial frequencies

All protocols and scanners showed a shift in their NPS spectra towards the lower spatial frequencies when using IR compared to FBP (see Figure 4.6). The shift entails a change in the perceived noise structure from a finer graininess to a more coarse graininess. This indicates that the use of IR changes the appearance of the noise in the image, which is in agreement with studies like Löve *et al* [27] and Brænne *et al* [40], where the latter connects the shift in median value with a poorer image quality.

The shift in median values varies between the scanners, with Toshiba showing the greatest shift for all protocols, and Philips the smallest shift. This is in accordance with Löve *et al* [27], who also found that the shape of the NPS curve, and thus its median value, was least affected by Philips' iDose algorithm.

All of the scanners use different IR algorithms, which will affect the noise structure in different ways. The different shifts in median value could indicate that some scanners' systems affect the noise structure more than others. Each system also has its own way of labelling the amount of IR used in the reconstruction, so that choosing an ASIR-V level of 50% on GE, iDose level 3 of 7 on Philips, ADMIRE level 3 of 5 on Siemens, and the AIDR 3D "Standard" level on Toshiba, can result in different levels of noise reduction being used, even if they all represent medium values of IR in their respective systems.

Adaptive noise reduction

From the noise maps in Figures 4.7-4.9, it seems that the IR algorithms on GE, Philips and Siemens reduce the noise with a certain amount; the more noise there is in the FBP image, the more noisy will the corresponding IR image be. The spatial noise distribution in each IR image is also similar to the distribution for FBP, in that they both show more noise in the center of the phantom and less towards the periphery. This indicates that the noise has been reduced by approximately the same amount in the entire image, so that the relative differences in noise between phantom center and periphery is similar for both FBP and IR noise maps.

For Toshiba, all of the IR noise maps have a more similar noise level than for the other scanners, as seen in Figure 4.10. This indicates that the higher the noise level in an image is, the more noise reduction will be applied by the AIDR 3D algorithm on Toshiba. Also, the noise distribution as a band along the largest diameter of the phantom is only visible for FBP, and disappears with IR. This indicates that Toshiba's IR algorithm is more adaptive than for the other scanners, i.e. the amount of noise reduction applied is adapted to the noise level that is present in each part of the image.

5.6 Dose levels

The CTDI_{vol} showed large variations between the four scanners (see Figure 4.1). For all protocols the largest CTDI_{vol} value was used on the Philips scanner, while Toshiba gave the lowest value. For the 5mm protocols, which are both directly based on AAPM recommendations, the CTDI_{vol} used on Philips was more than three times as high as the CTDI_{vol} given on Toshiba. Using the AAPM protocol recommendations does thus not guarantee that patients will be exposed to similar radiation doses on different scanners.

5.7 Dose modulation

The ATCM systems on GE and Toshiba aim at maintaining a uniform noise level throughout a scan, defined by an operator specified noise index. Still, it is easy to recognize the shape of the phantom in the noise plots in Figures 4.4-4.5 for all scanners, also for GE and Toshiba. This indicates that even when a noise index is used with ATCM, there will be less SD noise in low attenuating areas, like the thin end section of the phantom, and more in high attenuating areas, like the thick middle section of the phantom. Merzan *et al* [16] have shown similar results using the same phantom.

A contributing factor to the noise decrease in the small and medium sized end sections compared to the large middle section of the phantom, could be that the SD noise was measured in an ROI with a fixed diameter of 140 mm (see Figure 3.3). The diameter of the ROI thus covered 84%, 70% and 60% of the phantom's D_y diameter in the small, medium and large phantom sections respectively. The ROI applied to the small phantom section will include more pixels from the phantom periphery compared to the ROIs applied in the large and medium sized sections. As was shown in the noise maps in Figures 4.7-4.10, more noise was present in the center of the phantom cross-section, and less noise towards the phantom edges. This could make the SD noise appear lower in the small and medium sized sections compared to the large section, because the ROI here will cover more of the low-noise areas close to the phantom edges.

For GE, Philips and Siemens, the noise curves show a dip in the transition from the small end section to the large middle section of the phantom. This is a result of online dose modulation, where the radiation dose for each rotation is based on the measured attenuation of the previous rotation. The dip indicates that the phantom was scanned in the negative z-direction in Figures 4.4-4.5, so that the first scanned part of the small phantom section receives a radiation dose based on the attenuation of the last scanned part of the large middle section. This will result in a higher dose, and thus less noise, than for the rest of the small section.

5.8 Spatial noise distribution

The spatial noise distribution visualized in the noise maps in Figures 4.7-4.10 for each scanner, corresponds with results from other studies done by Merzan *et al* [16] using the same phantom: noise on GE, Philips and Siemens decrease from the center of the phantom towards the periphery, and noise on Toshiba is distributed in a band across the largest diameter of the phantom. The difference in spatial noise distribution for Toshiba is attributed to its x-ray spectrum, which is softer compared to the other vendors. X-ray photons with lower energies will be more attenuated through the phantom, and cause more noise along the longest traversed distance. In addition to the x-ray spectrum, Toshibas angular ATCM in the xy-directions could play a role in the noise distribution

From the noise maps presented in this thesis, all IR algorithms seem to be reducing the image noise in every part of the images. However, a study from Dalehaug *et al* [39] have shown that this is not always the case. If an anthropomorphic phantom containing organ structures is imaged using IR, the noise is reduced more in uniform areas of the phantom, and less at the borders between structures with different attenuation. The ATCM phantom used in this thesis is made of a uniform material without structures, and thus lacks transitions and edges between materials with different attenuation. Because of this, comparing our noise maps obtained with FBP and IR will not be representative of the noise reduction that would be present in clinical images, as they will contain different organ and tissue structures.

5.9 Know your scanner

Ideally, all CT scanners on the market would provide the same image quality for the same dose, but this is difficult to obtain in practice. Vendors publish and share some documentation describing the operating principles of their scanners, but there are still aspects that appear as a "black box" where the working mechanisms are unknown, and not always intuitive, to the operator. Many solutions used in different CT scanners will be patent protected, and not available to the public to ensure that competing companies cannot copy innovative solutions. This makes the task of standardizing exposure parameters for protocols used on different scanners challenging.

As have been demonstrated through this thesis, different scanners perform in different ways, even when the operator aims for similar behavior. Some of the differences discovered for the four scanners used in this thesis was how GE was the only scanner that reduced the dose when using IR, how Philips adjusted the rotation time automatically, how Toshiba interprets the application of exposure parameter inputs from the operator, and the adaptive nature of the IR algorithm used on Toshiba.

Each CT scanner is a complex machinery, put together of a large number of parts and components, and equipped with its own software, systems and algorithms. Differences in the x-ray tubes, detector arrays, filters and reconstruction kernels are just a few examples of elements that affects the working mechanisms of a CT scanner. In addition to this, each vendor has their own take on how each scan should be automated, what the operator should be able to control, and what should happen automatically "behind the scenes". All of these elements, and many more, take part in making up the complex task of predicting the outcome of using a certain set of exposure and reconstructing parameters. It therefore comes as no surprise that optimized guidelines for what exposure parameters to use can only be made if one is familiar with the scanner in question. In order to be able to provide the most optimized procedure possible, it is important to know the details of how your scanner works.

5.10 Suggestions for improvement

In the AAPM protocol recommendations, no recommendations were available for the GE Revolution scanner. This is because the scanner was not yet on the market when the recommendations were published in 2014. For this reason, the protocols used on GE were based on the most recent AAPM recommendations available for a GE scanner, namely the Discovery CT750 HD (w/ASIR). Since the recommendations were not tailored to fit the Revolution scanner specifically, the obtained results will be affected by the differences between the two scanners. If AAPM at a later point publish recommendations for the GE Revolution scanner, these recommendations should be used when doing similar analysis of radiation dose and image noise behavior on the same scanner. Still, the obtained results on GE seem reasonable, so it is assumed that the tendencies observed for radiation dose and image noise are still reliable.

On each of the four scanners, only one scan was performed with each of the six protocols. The tendencies observed on each scanner can thus give an indicator of how the scanner behaves, but can not be tested for statistical significance. If more scans were per-

formed with each protocol on each scanner, the statistical accuracy of the measurements would be improved. Still, the results observed in this thesis can give a valuable indication of what to expect of the radiation dose and image noise behavior on each scanner when the slice thickness is reduced.

In this thesis, only CT Thorax/Abdomen/Pelvis protocols were used. Other protocols will use different reconstruction algorithms to optimize the diagnostic quality of the images with respect to the structure of interest. A protocol used to image e.g. the lungs will use a sharper reconstruction algorithm compared to the Thorax/Abdomen/Pelvis, and this will affect the image noise. Thus, the results presented in this thesis would not necessarily be identical if another protocol than the Thorax/Abdomen/Pelvis was used as a basis.

As mentioned in Section 5.7, the ROIs used to calculate the SD noise had a fixed diameter. This could make the noise calculated in the small and medium sized sections appear lower relative to the results obtained in the large phantom section. A possible expansion of the work presented would be to account for this effect by using an ROI with a diameter set relative to the phantom's dimensions. If an ROI with a diameter of e.g. 60% of D_y in each phantom section was used, the area covered by the ROI is expected to show a more similar spatial noise distribution in each phantom section. This could make the measured noise level in the three phantom sections more similar.

To further assess the performance of the IR algorithms used on each scanner, it would be usefull to perform several scans of an anthropomorphic phantom to be able to create noise maps for each protocol with images containing structures. In this way it would be possible to evaluate how the different IR algorithms reduces noise along borders of differently attenuating material. This is more clinically relevant than looking at the noise reduction in a uniform material, which was the case for the ATCM phantom.

This thesis focused primarily on analyzing the results obtained in the large middle section of the phantom. A natural expansion of the work presented would be to do further analysis on the images of the two end sections as well. It would be especially interesting to compare noise maps between the different phantom sections for a single scan, and see if they show a similar noise reduction between each section as was found for the SD noise. This could give an indication of how much the fixed ROI size affected the SD noise.

Chapter 6

Conclusion

This thesis investigated the effects on radiation dose and image noise of the newly standardized image slice thickness reduction from 5 mm to 3 mm for CT Thorax/Abdomen/Pelvis protocols in Helse Vest.

Brooks' formula proved to give accurate predictions for the behavior of radiation dose and image noise when the image slice thickness was reduced. This was the case for protocols using both FBP and IR as image reconstruction methods, indicating that the 40 year old formula can still be used as a starting point when estimating changes in dose and noise on modern scanners. For this reason, Helse Vest is advised to keep using the estimates made with Brooks' formula for the standardization project.

The different scanners used in this thesis have displayed differences in their working mechanisms. This calls for Helse Vest to proceed carefully when pursuing a further standardization of exposure parameters, taking into account the particular specifications of each scanner. Particularly, they are advised to pay attention to the following three behaviors:

- The application of IR can give either a benefit in the form of a radiation dose reduction, as was seen for the GE scanner, or as an improvement of the image quality, as was seen for the Philips, Siemens and Toshiba scanners. This will affect how the ATCM index should be chosen to obtain the desired image quality.
- The IR algorithm on Toshiba adapt the amount of applied noise reduction according to the noise level present in the image. This was not the case for GE, Philips and Siemens.
- The Toshiba scanner applies the chosen noise index to a pre-defined slice thickness of 5 mm, regardless of the reconstructed slice thickness chosen by the operator. This behavior needs to be accounted for when choosing the appropriate noise index for a protocol on the Toshiba scanner.

Bibliography

[1] A. Almén, E. G. Friberg, A. Widmark, and H. M. Olerud, "Trends in examination frequency and collective effective dose to the population. StrålevernRapport 2010:12," Language: Norwegian, Norwegian Radiation Protection Authority, Østerås, 2010.

[2] Helse Vest. (Sep. 22, 2016). Organisering og kart, Helse Vest, [Online]. Available: `https://helse-vest.no/Documents/Om%20oss/Detaljert_kart_foretak_sjukehus.pdf` (visited on 04/23/2018).

[3] The American Association of Physicists in Medicine. (Feb. 20, 2014). Routine Adult Chest-Abdomen-Pelvis CT Protocol, [Online]. Available: `https://www.aapm.org/pubs/CTProtocols/documents/AdultRoutineChestAbdomenPelvisCT.pdf` (visited on 04/17/2018).

[4] Oxford English Dictionary. (2018). Tomography, [Online]. Available: `https://en.oxforddictionaries.com/definition/tomography` (visited on 02/15/2018).

[5] T. M. Buzug, *Computed tomography: from photon statistics to modern cone-beam CT*. Springer Science & Business Media, 2008.

[6] E. J. Hall and A. J. Giaccia, *Radiobiology for the Radiologist*. Lippincott Williams & Wilkins, 2006.

[7] W. R. Hendee and M. K. O'Connor, "Radiation risks of medical imaging: Separating fact from fantasy," *Radiology*, vol. 264, no. 2, pp. 312–321, 2012.

[8] A. Widmark, E. G. Friberg, H. M. Olerud, R. D. Silkorset, M. Solberg, K. Wikan, G. Saxebøl, and H. Kofstadmoen, "Guidance for use of medical X-ray and MR equipment. Guidance to "Regulations for radiation protection and use of radiation". Guidance No. 5.," Norwegian, Norwegian Radiation Protection Authority, Østerås, 2005.

[9] N. B. Smith and A. Webb, *Introduction to medical imaging: physics, engineering and clinical applications*. Cambridge university press, 2011.

[10] Philips Healthcare, *Clinical confidence in action. Philips Ingenuity Core128 specifications*, 2012.

[11] Toshiba Medical Systems Corporation, *Aquilion Prime. High-end CT system for your clinical needs today and in the future.* 2013.

[12] Siemens Healthcare. (2018). Simulation of x-ray spectra, [Online]. Available: https://www.oem-xray-components.siemens.com/x-ray-spectra-simulation (visited on 02/19/2018).

[13] E. L. Ridley. (Aug. 23, 2013). Interactive reconstruction of raw CT data: The next frontier? [Online]. Available: https://www.auntminnie.com/index.aspx?sec=ser&sub=def&pag=dis&ItemID=104252 (visited on 02/15/2018).

[14] C. H. A. Murphy. (2005-2018). Motion artifact, Radiopedia, [Online]. Available: https://radiopaedia.org/articles/motion-artifact-2 (visited on 05/18/2018).

[15] G. Dougherty, *Digital image processing for medical applications*. Cambridge university press, 2009.

[16] D. Merzan, P. Nowik, G. Poludniowski, and R. Bujila, "Evaluating the impact of scan settings on automatic tube current modulation in CT using a novel phantom," *The British journal of radiology*, vol. 90, Mar. 8, 2016.

[17] The ImPACT group. (2002). RSNA 2002: what's new in CT, [Online]. Available: http://www.impactscan.org/rsna2002.htm (visited on 05/18/2018).

[18] M. R. Bruesewitz, L. Yu, T. J. Vrieze, J. M. Kofler, and C. H. McCollough, *Smart mA - Automatic Exposure Control (AEC): Physics Principles and Practical Hints*, Mayo Foundation for Medical Education and Research, 2008.

[19] Philips Healthcare, *Patient-centered CT imaging: New methods for patient-specific optimization of image quality and radiation dose*, 2012.

[20] S. L. Rego, L. Yu, M. R. Bruesewitz, T. J. Vrieze, J. M. Kofler, and C. H. McCollough, *CARE Dose4D CT Automatic Exposure Control System: Physics Principles and Practical Hints*, 2007.

[21] E. Angel, *SureExposure - Low Dose Diagnostic Image Quality*, Toshiba America Medical Systems, Inc., 2012.

[22] K. Birdwell and M. Rodts. (Feb. 23, 2017). Anatomical planes of the body, [Online]. Available: https://www.spineuniverse.com/anatomy/anatomical-planes-body (visited on 05/18/2018).

[23] Hellerhoff. (Sep. 14, 2017). Legionellenpneumonie in der computertomographie in 3 ebenen. German, [Online]. Available: https://commons.wikimedia.org/wiki/File:Legionellenpneumonie_44jm_-_CT_LF_ax_cor_sag_-_0001.jpg (visited on 04/25/2018).

[24] A. C. Mamourian, *CT Imaging: practical physics, artifacts, and pitfalls*. Oxford University Press, 2013.

[25] S. W. Smith, *The Scientist and Enigneer's Guide to Digital Signal Processing*. California Technical Publisher, 1997. [Online]. Available: http://www.dspguide.com/ (visited on 05/04/2018).

[26] M. Beister, D. Kolditz, and W. A. Kalender, "Iterative reconstruction methods in X-ray CT," *Physica Medica: European Journal of Medical Physics*, vol. 28, no. 2, pp. 94–108, 2012.

[27] A. Löve, M. Olsson, R. Siemund, F. Stålhammar, I. Björkman-Burtscher, and M. Söderberg, "Six iterative reconstruction algorithms in brain CT: a phantom study on image quality at different radiation dose levels," *The British journal of radiology*, vol. 86, no. 1031, 2013.

[28] V. Kisic and A. Murphy. (2005-2018). Windowing (CT), [Online]. Available: https://radiopaedia.org/articles/windowing-ct (visited on 02/09/2018).

[29] The Phantom Laboratory. (2017). Catphan 600, Modules, [Online]. Available: https://www.phantomlab.com/catphan-600 (visited on 01/30/2018).

[30] T. S. Curry, J. E. Dowdey, and R. C. Murry, *Christensen's physics of diagnostic radiology*. Lippincott Williams & Wilkins, 1990.

[31] P. Sprawls, *Computed tomography image quality optimization and dose management*. [Online]. Available: http://www.sprawls.org/resources/CTIQDM/ (visited on 05/25/2018).

[32] K. L. Boedeker, V. N. Cooper, and M. F. McNitt-Gray, "Application of the noise power spectrum in modern diagnostic MDCT: part I. Measurement of noise power spectra and noise equivalent quanta," *Physics in Medicine & Biology*, vol. 52, no. 14, p. 4027, 2007.

[33] H. D. Nagel, "CT parameters that influence the radiation dose," in *Radiation Dose from Adult and Pediatric Multidetector Computed Tomography*, D. Tack and P. A. Gevenois, Eds. Springer, 2007, ch. 4.

[34] M. F. McNitt-Gray, "AAPM/RSNA Physics Tutorial for Residents: Topics in CT," *RadioGraphics*, vol. 22, no. 6, pp. 1541–1553, 2002. [Online]. Available: https://doi.org/10.1148/rg.226025128 (visited on 05/18/2018).

[35] E. Andersen, *Dose distribution in CT scan*, Nov. 13, 2015. [Online]. Available: https://www.youtube.com/watch?v=ZquhJhv8cys (visited on 05/18/2018).

[36] The Phantom Laboratory, *CCT228 ATCM Phantom Manual*, 2017.

[37] W. S. Rasband. (1997-2018). Imagej, National Institutes of Health, [Online]. Available: https://imagej.nih.gov/ij/ (visited on 05/20/2018).

[38] E. Wasbø, *ImageQC - Quality Control in medical imaging*. [Online]. Available: https://github.com/EllenWasbo/ImageQC (visited on 04/19/2018).

[39] I. Dalehaug, K. N. Bolstad, D. Aadnevik, S. Flatabø, and H. E. S. Pettersen, "Admire vs. Safire: Objective comparison of CT reconstruction algorithms and their noise properties," *arXiv preprint arXiv: 1708.09616*, 2017. [Online]. Available: https://arxiv.org/abs/1708.09616 (visited on 05/07/2018).

[40] K. R. Brænne, L. I. Flinder, M. A. Martiniussen, K. Jensen, C. H. Reisse, L. Julsrud, and A. C. Martinsen, "A liver phantom study: Ct radiation dose reduction and different image reconstruction algorithms affect diagnostic quality," *Journal of computer assisted tomography*, vol. 40, no. 5, pp. 735–739, 2016.

Appendix A

AAPM protocol recommendations

Settings recommended by AAPM for each scanner used in this experiment is shown in Figure A.1. Notice that no recommendations were available for the GE Revolution scanner, so the protocol specifications for this scanner was based on the AAPM recommendations for the newest GE scanner available, namely the Discovery CT750 HD (w/ASIR).

GE	Discovery CT750 HD (w/ASIR) **
Scan Type	Helical
Rotation Time (s)	0.5
Detector Configuration	64 x 0.625 mm (40 mm, 8i)
Pitch	1.375
Table Feed/Interval (mm)	55.0
kV	120
Average mA	300
Auto-mA range	100-750
Noise Index (NI)*	35.42
SFOV	Large
ASiR	SS50

RECON 1

Plane	Axial; DMPR create thick Sag/Cor reformat
Algorithm	Stnd
Recon Mode	Plus
Thickness (mm)	0.625
Interval (mm)	0.625
ASiR	SS50

SIEMENS	Definition Flash (dual source, 128-slice)
Software version	VA44
Scan mode	Spiral
Tube voltage (kV)*	120
Qual. Ref. mAs (QRM)	210/150***
Rotation time (s)	0.5
Acq. (Detector Configuration)	**128 × 0.6 mm (64 x 0.6 mm = 38.4 mm)
Pitch	0.6
Dose modulation	CARE Dose4D

RECON 1

Kernel	B30f/I30f***
Slice (mm)	5.0
Slice increment (mm)	5.0

PHILIPS	Ingenuity CT
Scan Type	Helical
Rotation Time (s)	0.75
Collimation	64 × 0.625 mm
Coverage (mm)	40
kV	120
mAs (mAs/slice) @ water equivalent diameter	DoseRight (200 mAs @ 33 cm Reference OR 200 mAs @ DRI = 24)*, 3D Modulation
DoseRight ACS	ON
Pitch	1.1
FOV (mm)	350-500
SP Filter	Yes
Adaptive Filter	Yes
Resolution Setting	Standard

RECON 1

Type	Axial
Filter	B/C
Thickness (mm)	5
Increment (mm)	5

TOSHIBA	AqPRIME
Arterial Chest/Abdomen Pelvis	
Scan Type	Helical
Rotation Time (s)	0.5
Detector Configuration	80 x 0.5
Pitch	Std (0.813)
Speed (mm/rot)	32.5
kV	120
mA	SURE Exposure
SURE Exposure	Std (SD = 12.5)
Minimum & Maximum mA	80 & 500
SFOV	LFOV
Breath-hold	Inspiration

RECON 1

Type	Axial
SURE IQ setting	Body Std Axial
Thickness (mm)	5
Interval (mm)	5
DFOV (cm)	400

Figure A.1: The settings recommended by AAPM [3] on which the protocols used in this thesis are based.

Appendix B

Noise power spectra

The normalized NPS curves for each protocol used on the four scanners are shown in Figure B.1.

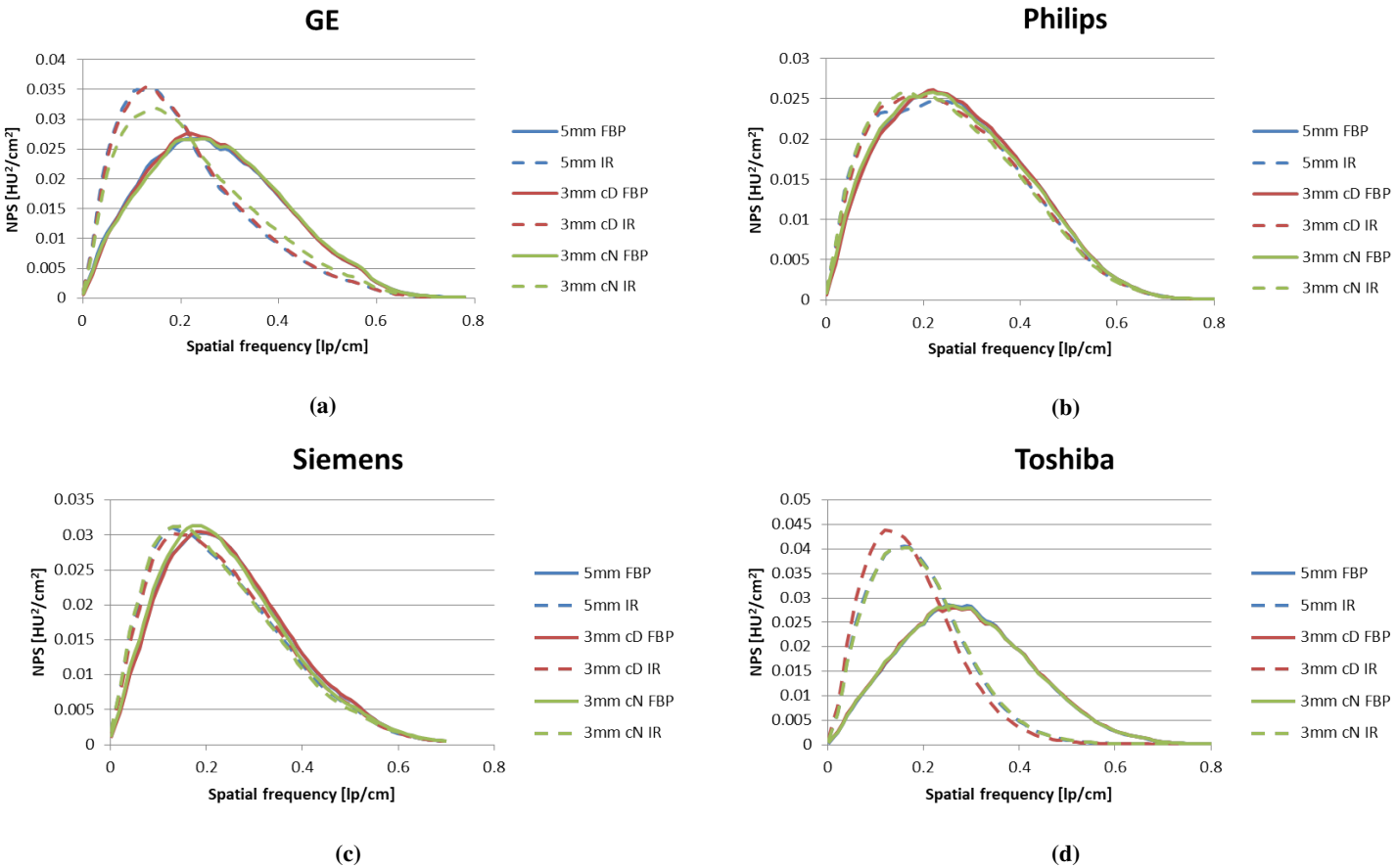

Figure B.1: Normalized NPS curves for each protocol on the **(a)** GE, **(b)** Philips, **(c)** Siemens and **(d)** Toshiba scanner.

Appendix C

Python script for extracting mAs curves

```
# -*- coding: utf-8 -*-
"""
Created on Tue Jan 16 14:14:52 2018

@author: daaa (Daniel Aadnevik)
Edited by Anette Guleng spring 2018
"""

""" Dosemodulering CT Haukeland Universitetssjukehus """

# Import packages
import pydicom
import os
import xlsxwriter as xl

# Change to folder
folder = "Path\to\folder\containing\image\folders"
os.chdir(folder)
files = os.listdir(folder)

x_list = []
y_list = []

# Create Excel file
workbook = xl.Workbook("Output_data.xlsx")
```

```
for element in files:

    # Write a header with the appropriate tags
    worksheet = workbook.add_worksheet(name=element)
    worksheet.write('E1','Z-posisjon [mm]')
    worksheet.write('F1','mAs')

    z_position = []
    mAs_list = []

    # Change to the folder containing images
    new_folder = folder + "\\" + element
    os.chdir(new_folder)
    dicom_images = os.listdir(new_folder)

    n = 2
    for x in dicom_images:
        ds = pydicom.read_file(x,stop_before_pixels=True)
        manufacturer = ds[0x8, 0x70].value

        # Getting identification parameters for each set of images
        if(n == 5):
            model = ds[0x8, 0x1090].value
            SliceThickness = ds[0x18, 0x50].value
            kVp = ds[0x18, 0x60].value
            exposureTime = ds[0x18, 0x1150].value
            convKernel = ds[0x18, 0x1210].value

            worksheet.write('A1', str(manufacturer) + ' ' +
                str(model))
            worksheet.write('A2', 'Slice thickness: ' +
                str(SliceThickness) + ' mm')
            worksheet.write('A3', 'kVp: ' + str(kVp))
            worksheet.write('A4', 'Exposure time: ' +
                str(exposureTime) + ' ms')
            worksheet.write('A5', 'Convolution kernel: ' +
                str(convKernel))

            # Getting IR level
            if "philips" in manufacturer.lower():
                try:
                    iDoseNumber = int(ds[0x1F7, 0x109B].value)
                except:
                    iDoseNumber = 0
                worksheet.write('A6', 'iDoseNumber: ' +
```

```
                str(iDoseNumber))

        elif "toshiba" in manufacturer.lower():
            try:
                AIDR3D = str(ds[0x7005, 0x100B].value).strip()
            except:
                AIDR3D = "ORG"
            worksheet.write('A6', 'AIDR3D: ' + str(AIDR3D))

        elif 'siemens' in manufacturer.lower():
            # Checks if kernel is a str
            if type(convKernel) != type("str"):
                kernel = "_".join(convKernel)
            if "b" in kernel.lower():
                worksheet.write('A6', 'ADMIRE: FBP')
            else:
                worksheet.write('A6', 'ADMIRE ' + str(kernel))

        elif 'ge medical systems' in manufacturer.lower():
            try:
                ASIR = ds[0x53, 0x1043].value
            except:
                ASIR = 0
            worksheet.write('A6', 'ASiR-V: ' + str(ASIR))

    # Getting current slice location
    SliceLocation = ds[0x20, 0x1041].value

    if "ge" in manufacturer.lower():
        # Calculating mAs from Exposure time and
        # X-ray tube current
        mAs = (ds[0x18, 0x1150].value *
            ds[0x18, 0x1151].value / 1000)
    else:
        # Getting mAs directly from Exposure
        mAs = ds[0x18, 0x1152].value

    # Write the slice location (z) and mAs to each column
    worksheet.write('E' + str(n),str(SliceLocation))
    worksheet.write('F' + str(n),str(mAs))

    # Get ready for the next column
    n += 1

    # Add the slice location and mAs to their respective lists
```

```
            z_position.append(float(SliceLocation))
            mAs_list.append(float(mAs))

        # Add the list of slice location and mAs for the
        # entire folder to x and y
        x_list.append(z_position)
        y_list.append(mAs_list)

        # Change back to original folder and get ready for
        # the next folder
        os.chdir(folder)

workbook.close()
```

Appendix D

Python script for creating noise maps

D.1 Main file

```
# -*- coding: utf-8 -*-
"""
Created by Helge Pettersen.
Edited by Anette Guleng, spring 2018
"""

import os
import dicom
import numpy as np
import matplotlib.cm as cm
import matplotlib.pyplot as plt
from scipy.signal import medfilt
from math import sqrt
from mpl_toolkits.axes_grid1 import make_axes_locatable

from matplotlib.backends.backend_agg import \
    FigureCanvasAgg as FigureCanvas
from matplotlib.figure import Figure

from myFunctions_kopi import *

folder = 'path\to\folder\containing\images'
kernels = os.listdir(folder)
print("Kernels: {}", kernels)
```

```
nImages = 50 # Number of images

image = {}
counter = {}
for kernel in kernels:
    image[kernel] = [False]*nImages
    counter[kernel] = 0

for root, dirs, files in os.walk(folder):
    for file in files:

        ds = dicom.read_file(root + "\\" + file)
        pixel_array = ds.pixel_array
        rescaleSlope = eval(str(ds.RescaleSlope))
        rescaleIntercept = eval(str(ds.RescaleIntercept))
        pixel_array = (np.copy(pixel_array) * rescaleSlope
                       + rescaleIntercept)
        kernel = ds.ConvolutionKernel

        IRLevel = getIRLevel(ds)

        image_size = np.shape(pixel_array)

        # Checks if kernel is a str
        if type(kernel) == type("str"):
            kernel = "%s_%s" % (str(ds.ConvolutionKernel),
                                IRLevel)
        elif type(kernel) != type("str"):
            kernel = "_".join(ds.ConvolutionKernel)

        # Define ROI
        dx = 420
        dy = 300
        yfrom = 100
        xfrom = 45

        imgROI = (np.copy(pixel_array)
                    [yfrom:yfrom+dy, xfrom:xfrom+dx])
        imgROI - np.mean(imgROI)
        roi_size = np.shape(imgROI)[0]
        image[kernel][counter[kernel]] = np.copy(imgROI)

        counter[kernel] += 1
```

```
print "Finished creating images."

n = dy
m = dx

kernelsize = 11
kernelsize_side = (kernelsize - 1) / 2

nCovi = {}
std = {}
values = np.zeros([n,m,nImages])

for kernel in kernels:
    nCovi[kernel] = np.zeros([n,m])
    std[kernel] = np.zeros([n,m])

wmin_nCovi, wmax_nCovi = getWindow('nCovi')
wmin_std, wmax_std = getWindow('std')

for kernel in kernels:

    print "\n\nCalculating nCovi for %s..." % kernel

    for x in range(n):
        for y in range(m):
            values[x,y] = [image[kernel][k][x,y]
                           for k in range(nImages)]

    print "Size of vector: %.2f MB." % (float(values.nbytes)
                                        /1e6)

    print "Finished preparing %dx%d image vector." % (m,n)

    for x in range(n):
        for y in range(m):

            xyvalues = np.copy(values[x,y])

            xjfrom = max(0, x - kernelsize_side)
            xjto = min(n, x + kernelsize_side)

            yjfrom = max(0, y - kernelsize_side)
            yjto = min(m, y + kernelsize_side)

            std[kernel][x,y] = sqrt(np.std(xyvalues))
```

```
    print ("Finished␣calculating␣nCovi␣for␣kernel␣%s.␣"
           + "Plotting..." % kernel)

    del values
    values = np.zeros([n,m,nImages])


# Adjust red level in noise image
totmin = 0
totmax = 4

for kernel in kernels:
    imgmin = np.min(std[kernel])
    imgmax = np.max(std[kernel])

    if not totmin:
        totmin = imgmin

    if not totmax:
        totmax = imgmax

for kernel in kernels:

    ticks = [totmin*1.2, (totmax*0.8+totmin*1.2)/2.,
             totmax*0.8]

    plt.imshow(std[kernel], interpolation = 'nearest',
               cmap=cm.gist_heat, vmin=ticks[0], vmax=ticks[-1])

    ax = plt.gca()

    ax.axes.get_yaxis().set_ticks([])
    ax.axes.get_xaxis().set_ticks([])

    divider = make_axes_locatable(ax)
    cax = divider.append_axes("right", size="5%", pad=0.05)

    CB = plt.colorbar(cax=cax)
    ticklabels = ["%.1f␣HU" % x for x in ticks]

    plt.suptitle("Inter-image␣standard␣deviation␣for␣{}"
                 .format(kernel))

    CB.set_ticks(ticks)
```

```
    CB.set_ticklabels(ticklabels)

    plt.savefig('output_G\\3mm_CN0-4_std_%s.png' % kernel,
                bbox_inches='tight', dpi=250)

    plt.close()
```

D.2 Functions

```
# -*- coding: utf-8 -*-
"""
Created on Tue Apr 22 10:56:56 2014

@author: rttn
Edited by Anette Guleng, spring 2018
"""
import datetime, time
import dicom.UID
from dicom.dataset import Dataset, FileDataset
import numpy as np

import matplotlib.pyplot as plt

def write_dicom(ds, pixel_array,filename, slope, offset, signed):
    """
    INPUTS:
    pixel_array: 2D numpy ndarray.  If pixel_array is larger
        than 2D, errors.
    filename: string name for the output file.
    """

    ds.RescaleSlope = int(slope)
    ds.RescaleIntercept = int(offset)

    ds.Columns = pixel_array.shape[0]
    ds.Rows = pixel_array.shape[1]

    if not signed:
        if pixel_array.dtype != np.uint16:
            pixel_array = pixel_array.astype(np.uint16)
    else:
        if pixel_array.dtype != np.int16:
            pixel_array = pixel_array.astype(np.int16)

    ds.PixelData = pixel_array.tostring()
```

```
    ds.save_as(filename)
    return


def SaveFigureAsImage(fileName,fig=None,**kwargs):
    ''' Save a Matplotlib figure as an image without borders
        or frames.
       Args:
            fileName (str): String that ends in .png etc.

            fig (Matplotlib figure instance): figure you want
                to save as the image
        Keyword Args:
            orig_size (tuple): width, height of the original
                image used to maintain aspect ratio.
    '''
    fig_size = fig.get_size_inches()
    w,h = fig_size[0], fig_size[1]
    fig.patch.set_alpha(0)
    # Aspect ratio scaling if required
    if kwargs.has_key('orig_size'):
        w,h = kwargs['orig_size']
        w2,h2 = fig_size[0],fig_size[1]
        fig.set_size_inches([(w2/w)*w,(w2/w)*h])
        fig.set_dpi((w2/w)*fig.get_dpi())
    a=fig.gca()
    a.set_frame_on(False)
    a.set_xticks([]); a.set_yticks([])
    plt.axis('off')
    plt.xlim(0,h); plt.ylim(w,0)
    fig.savefig(fileName, transparent=True,
                bbox_inches='tight', pad_inches=0)


def getWindow(windowName):
    if not windowName in ('lung', 'abdomen', 'subtraction',
                          'nCovi', 'std'):
        print "Could not find window %s, exiting." % windowName
        raise

    if windowName == "lung":
        window = 1600
        level = -400
    elif windowName == "abdomen":
```

```
        window = 350
        level = 50
    elif windowName == 'subtraction':
        window = 35
        level = 0
    elif windowName == 'nCovi':
        window = 25
        level = 2.5
    elif windowName == 'std':
        window = 8
        level = 2.15

    wmin = level - window / 2.
    wmax = level + window / 2.

    return wmin, wmax


def getIRLevel(ds):
    manufacturer = ds.Manufacturer
    kernel = ds.ConvolutionKernel

    if "philips" in manufacturer.lower():
        try:
            iDoseNumber = int(ds[0x1F7, 0x109B].value)
        except:
            iDoseNumber = 0

        if iDoseNumber == 0:
            IRLevel = 0
        elif iDoseNumber == 1:
            IRLevel = 1
        elif iDoseNumber == 3:
            IRLevel = 2
        elif iDoseNumber == 5:
            IRLevel = 3
        else:
            IRLevel = -1
#
    elif "toshiba" in manufacturer.lower():
        try:
            AIDR3D = str(ds[0x7005, 0x100B].value).strip()
        except:
            AIDR3D = "ORG"
```

```
            AIDR3D = "ORG"

        AIDR3D_names = {"ORG" : 0,
                        "AIDR␣3D␣MILD" : 1,
                        "AIDR␣3D␣STR" : 2,
                        "AIDR␣3D␣STD" : 3}

        IRLevel = AIDR3D_names[AIDR3D]

    elif 'siemens' in manufacturer.lower():
        # B30f, I30f_1, I30f_3, I30f_5
        # Checks if kernel is a str
        if type(kernel) != type("str"):
            kernel = "_".join(kernel)
        if "b" in kernel.lower():
            IRLevel = 0
        elif "_1" in kernel.lower():
            IRLevel = 1
        elif "_3" in kernel.lower():
            IRLevel = 2
        elif "_5" in kernel.lower():
            IRLevel = 3
        elif "_2" in kernel.lower():
            IRLevel = 1.5

    elif 'ge␣medical␣systems' in manufacturer.lower():
        try:
            ASIR = ds[0x53, 0x1043].value
        except:
            ASIR = 0

        if ASIR == 0:
            IRLevel = 0
        elif "40" in ASIR.lower():
            IRLevel = 2
        elif "50" in ASIR.lower():
            IRLevel = 2
        elif "100" in ASIR.lower():
            IRLevel = 3

    return IRLevel


def getROIdimensions(roiName, manufacturer="Siemens"):
    if not roiName in ('left', 'right', 'catphan', 'big',
```

```
                    'superbig', 'megabig', 'catphanbig',
                    'catphansmall'):
        print "Could not find dimensions for ROI %s, exiting." \
                                                    % roiName
        raise NameError(roiName)

    if manufacturer == "Philips":
        scaleFactor = 2
    else:
        scaleFactor = 1

    if manufacturer == "Toshiba":
        imageFlipSize = 512
        flipFactor = -1
        dFactor = 1

    else:
        imageFlipSize = 0
        flipFactor = 1
        dFactor = 0

    if roiName == "left":
        xfrom = 80
        yfrom = 170
        d = 130

    elif roiName == 'right':
        xfrom = 300
        yfrom = 160
        d = 104

    elif roiName == 'big':
        xfrom = 150
        yfrom = 100
        d = 195

    elif roiName == 'superbig':
        xfrom = 106
        yfrom = 106
        d = 300

    elif roiName == 'megabig':
        xfrom = 32
        yfrom = 32
        d = 448
```

```
    elif roiName == 'catphansmall':
        xfrom = 192
        yfrom = 192
        d = 128 * scaleFactor

    elif roiName == 'catphan':
        xfrom = 128
        yfrom = 128
        d = 256

    elif roiName == 'catphanbig':
        xfrom = 64
        yfrom = 64
        d = 384

    return ((imageFlipSize - dFactor * d + flipFactor * xfrom) *
            scaleFactor,
            (imageFlipSize - dFactor * d + flipFactor * yfrom) *
            scaleFactor, d * scaleFactor)
```

Appendix E

Deviations between displayed and measured CTDI_{vol} values

Table E.1 shows an excerpt from the last annual control report from Helse Vest, where the CTDI_{vol} displayed on the operator console is compared to measured CTDI_{vol} values for the scanners used in this thesis. For all scanners, the deviation is $\pm 10\%$ or less.

Table E.1: Deviation of displayed and measured CTDI_{vol} values for the CT scanners used in this thesis. Data from quality control measurements in Helse Vest.

Scanner	Displayed CTDI_{vol}	Measured CTDI_{vol}	Deviation
GE (HDS)	45.3	44.2	-2.4%
Philips (KiH)	16.4	15.5	-6%
Siemens (HUS)	31.14	27.83	-10.6%
Toshiba (HUS)	22.9	21.5	-6%